

Efficient Hamiltonian Simulation: A Utility Scale Perspective for Covalent Inhibitor Reactivity Prediction

Marek Kowalik¹, Sam Genway¹, Vedangi Pathak^{2,3}, Mykola Maksymenko⁴,
Simon Martiel⁵, Hamed Mohammadbagherpoor², Richard Padbury²,
Vladyslav Los^{4,6}, Oleksa Hryniv⁴, Peter Pogány⁷, Phalgun Lolur^{1*}

¹ Capgemini Quantum Lab

² IBM T. J. Watson Research Center, Yorktown Heights, NY

² Department of Physics and Astronomy at University of British Columbia

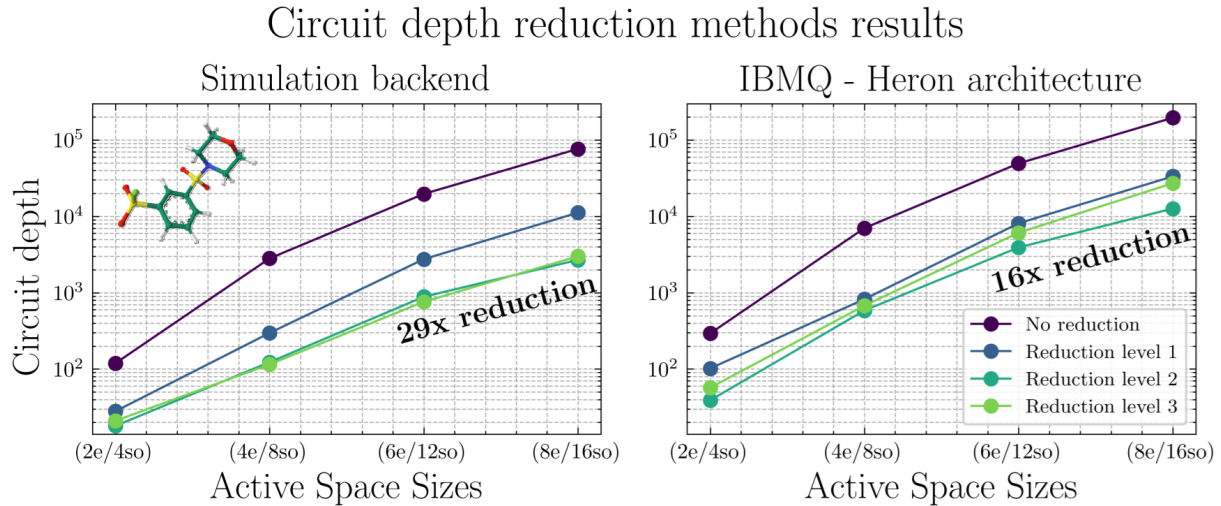
⁴ Haiqu Inc.

⁵ IBM Quantum, IBM France Lab, Orsay, France

⁶ Institute for Quantum Information, RWTH Aachen University

⁷ GSK Medicines Research Centre, Gunnels Wood Road, Stevenage, Hertfordshire SG1 2NY, United Kingdom

* Corresponding author - phalgun.lolur@capgemini.com



Mean circuit depth for different reduction methods applied on an exemplary molecule simulation circuit for 1 Trotter step. Circuits were transpiled on all-to-all connectivity with Clifford + R_z set of gates (left figure) and IBM Heron R2 architecture (right figure) for 50 trails per each data point. The best reduction from all the methods and active spaces per each backend is annotated with a numerical value.

Abstract: Quantum computing applications in the noisy intermediate-scale quantum (NISQ) era demand algorithms capable of generating shallower circuits that are feasible to run on today’s quantum systems. This is a challenge, particularly for quantum chemistry applications, considering the inherent complexity of molecular systems. In this paper, we demonstrate advancements that expand the size of chemistry problems that can be run on today’s quantum systems by applying hardware-efficient approaches, such as Quantum-Centric Data-Driven Research and Development (QDDRD), optimized algorithms with reduced circuit depth, and execute the experiments with middleware-supported quantum error mitigation. We report up to a 29-fold reduction in circuit depth for covalent drug molecules, enabling Hamiltonian dynamics for reactivity predictions, assuming all-to-all connectivity of quantum hardware. When employed on IBMQ’s Heron architecture, we see up to a 16-fold reduction. The overarching impact of this work is that it highlights promising methods that allow researchers to explore the dynamics of commercially relevant chemistry on real quantum hardware via Hamiltonian simulation.

I. INTRODUCTION

Quantum chemistry simulation, famously discussed by Richard Feynman in 1981 [1], is seen as one of the most promising applications of quantum computing [2]. Specifically, electronic structure Hamiltonian simulations play a central role as a tool to extract chemistry insights from commercially relevant materials [3]. In the current noisy intermediate-scale quantum (NISQ) era, before error-corrected fault-tolerant quantum computers (FTQC) are available, the primary task of researchers is to frame commercially interesting use cases into scalable solutions that leverage today’s quantum computers [2]. Ideally, quantum computers should perform the parts of the overall calculation that are current bottlenecks for classical simulations, while the rest of the calculation can be treated classically. For quantum chemistry applications, this includes Hamiltonian simulation in a variety of forms [3].

Previously, small-scale chemistry systems, in terms of molecule and active space size, were examined to create simulation problems that could be explored on today’s quantum hardware [4]. However, recent progress has been made towards more accurate calculations of the electronic structure prediction (the ground and excited states) of larger quantum systems on current quantum computers [5]. This has been achieved with proper error mitigation techniques [5] and hybrid quantum-classical algorithms [6]. Recent examples using Sample-based Quantum Diagonalization to calculate the ground and excited states energies of iron-sulfur clusters with (54e, 36o) and (30e,20o) active spaces, respectively are described in detail in [5, 7, 8]. Conversely, simulating dynamics (the focus of this paper), which is essential to understanding molecular vibrations, complex molecular interactions, chemical reactions, and material properties, poses additional challenges. This is due to the complexity and longer simulation times needed to calculate the time evolution of the quantum system (quantum dynamics) via Hamiltonian simulation. This can lead to significantly larger circuit depths depending on the size, structure of the molecule, and active space selected for the study.

To identify and evaluate practical use cases for quantum computing, we need to push the capabilities of current hardware by simulating larger systems towards commercially relevant applications and to help understand how a solution will scale as the hardware improves. As the quality of quantum processing units (QPU) continues to progress, yielding quantum systems with smaller error rates, there is also significant effort and opportunity to optimize quantum algorithms [9, 10] by reducing circuit depths [11, 12] and the sampling overheads

required [2, 13–15] to perform Hamiltonian simulations on current quantum systems.

One of the frameworks leveraging Hamiltonian simulations towards practical use cases is Quantum-Centric Data-Driven R&D (QDDRD), which is provided in [4]. Such framework incorporates predictive modeling pipelines with machine learning (ML) models that rely on the outputs of quantum simulations, so-called ‘*quantum fingerprints*’. The advantage of such an approach is that, e.g. the reactivity prediction for covalent series drugs, as in the original paper, is shifted from excited-states estimation problem to the ML prediction based on Hamiltonian simulations. Predicting drug activity via computational chemistry alone (i.e. DFT and/or molecular dynamics) through the excited states energy estimation is computationally intensive or even intractable both for classical and quantum computers. ML provides a data-driven method that bypasses the computational bottleneck but presents a different challenge - ML models need to be trained on proper quantum features (i.e. mainly with the proper size of active space) to yield sufficient accuracy in the prediction. Those features are hard to obtain experimentally or to calculate by using classical computational methods alone. Therefore, we are exploring the potential of quantum computing to calculate features that can be used to enrich a feature set for drug activity prediction via ML. Currently, Hamiltonian simulation is challenging to perform on a quantum computer due to noise. We address this challenge in this paper by looking at the scalability of the Hamiltonian simulation approach after application of the circuit reduction techniques. After performing a series of hardware experiments on today’s systems, those results might be extrapolated towards larger active spaces either considering hardware roadmaps and QPUs of lower error levels or algorithmic improvements, which is possible in the proposed scope for quantum circuit reductions.

Also, the final objective (reactivity) is not analytically calculated with quantum computers but predicted with classical ML models, which may show robustness to systematic errors coming from runs on real quantum computers and algorithmic approximations.

In our investigation, we employed previous pharmaceutical implementations of quantum mechanics on targeted covalent drugs[4, 16], a field that has recently experienced considerable growth in research interest[17–19]. Unlike traditional small-molecule inhibitors, the mechanism of action of covalent drugs on protein targets involves two distinct steps: initially, the drug molecule forms a reversible complex with the target protein, followed by a covalent bond formation between a reactive moiety, or “warhead”, present on the drug molecule,

and a nucleophilic amino acid residue within the protein target. This covalent attachment can enhance drug potency, thereby reducing the necessary dosage and ensuring high specificity. Historically, the utility of covalent drugs can be traced back to aspirin, but their resurgence in pharmaceutical research has been fueled by advancements in chemoproteomic assays which facilitate proteome-wide studies.

In the domain of drug discovery, *in silico* methods, that encompass machine learning and molecular simulations, have attained significant prominence over the past four decades. This is largely due to a combination of vastly improved computational power on top of available experimental data for training models. These computational methodologies can facilitate more rapid and extensive assessments of drug-like compounds in comparison to *in vitro* experimentation. Despite these massive improvements, there are limitations to what computational methods can address given the problem size complexities, specifically for drug molecules. One of the central challenges in designing targeted covalent drugs is the prediction of warhead reactivity, a crucial factor in balancing drug potency and selectivity[20]. Thus, effective computational approaches to address this challenge are anticipated to substantially impact the field.

A specific series of chemical reactions that have been extensively analyzed for their reactivity and other associated properties involves sulfonyl fluoride (SO_2F) warheads, which predominantly target non-thiol containing amino acids such as lysine, serine, and tyrosine. Reactivity predictions in this context have been successfully achieved using density functional theory (DFT) calculations to ascertain the energy of the lowest occupied molecular orbital (LUMO) [16]. Conversely, for other warheads, like acrylamides, comprehensive DFT calculations focused on transition states are required to rank the reactivity of compounds in a manner consistent with empirical data[21]. In our previous study employing the DMET approach, we successfully projected a proxy for molecular reactivity using DMET with smaller active space compared to the previous DFT methodologies applied for LUMO calculations.

In this work, we propose a quantum circuit reduction setup for the Hamiltonian simulation, evaluate it on the commercially relevant molecules with the obtained reduction up to 15.5 times as the results, and assess further possibilities of cutting the circuit depth based on the evaluation of trade-off between predictive model accuracy and algorithmic approximation of the problem.

This paper is organized as follows: the Background Section II introduces the algorithm

for Hamiltonian simulation and names used circuit reduction methods, then the high-level description is provided for the QDDRD framework with Hamiltonian dynamics algorithm applied. In Section III, we describe the use case and experimental setup of the quantum simulations that include the circuit reduction methods used for PF. Subsequently, Section IV describes the computational details of the circuit reduction methods. Section V presents the Hamiltonian simulation results evaluated with an exemplary molecule using simulators and real quantum computers plus the ML model evaluation for reactivity prediction. This is followed by the Discussion VI and Conclusion Sections VII. Finally, the appendix includes the description of electronic energy dynamic simulations using product formulas (PF), discussions on the cost of Pauli String exponentiation gates, evaluations of qubit mapping algorithms, more detailed descriptions of the circuit reduction techniques, and additional results.

II. BACKGROUND

First, it is necessary to choose a specific Hamiltonian simulation method. There are a variety of Hamiltonian simulation approaches and methods to choose from. For this paper, the main focus is put on a real-time evolution problem which can be resolved using methods such as product formulas (PF) [22], quantum walks [23], fractional-query simulations [24], Taylor series (TS) [25] and quantum signal processing (QSP) [9]. The optimal method for large system sizes can be chosen based on gate complexity for which QSP might be the optimal choice for certain Hamiltonians [26, 27]. However, in the current era, PF is more flexible and efficient choice for smaller active space sizes due to its general simplicity (no large unitary control gates) and relatively shallow circuits that still lead to strong approximations (first-order formula with few trotter steps). QSP even for small systems usually requires deep circuits, impossible to run without quantum error correction. Furthermore, PF is more scalable than TS and QSP after applying accuracy empirical bounds [28] on a number of trotter steps, which was shown on 1D-spin lattice systems [27]. Additionally, to optimize experiments on larger active space sizes, methods to further reduce the circuit depths yielded by the PF can be applied. These methods include: Hamiltonian terms truncation, Clifford Decomposition and Transformation (CDAT) [29], and qubit tapering [30, 31]. Details of these methods and detailed results for the reduced circuits are provided in the Appendices.

A. QDDR framework

The quantum chemistry problem highlighted in this work is the reactivity prediction of a series of targeted covalent drug inhibitors using the ‘quantum features’ as described in [4]. Following on from this previous work, we perform predictions using the data-driven pipeline shown in Figure 1 that leverages gate-based quantum computers to calculate quantum features.

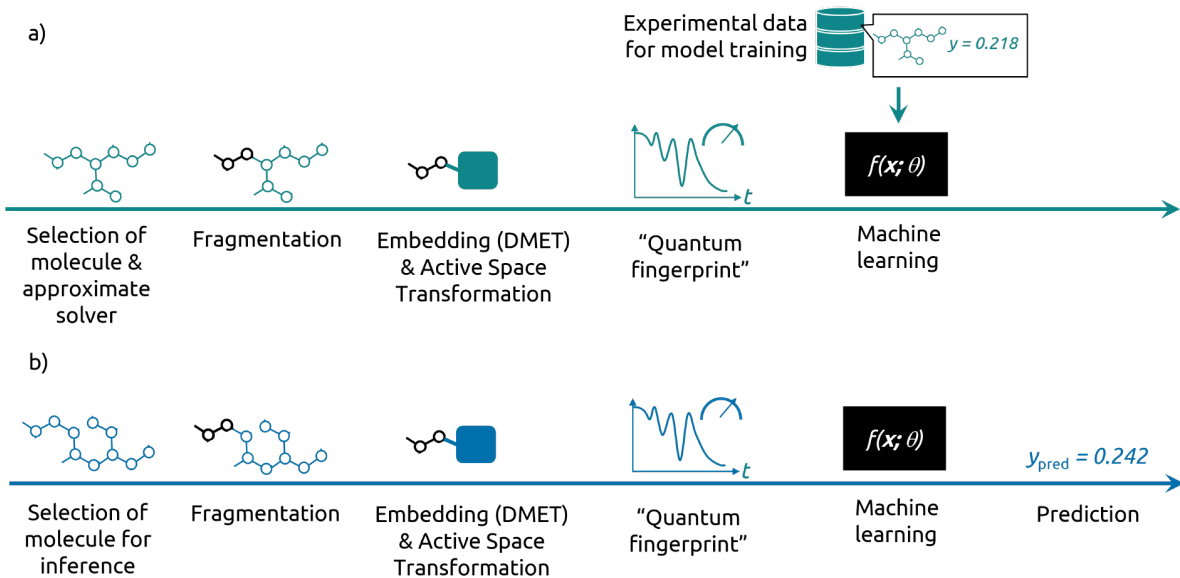


FIG. 1: *High-level representation of the data-driven pipeline used to predict molecule reactivities using quantum computers and ML. Training stage a) is conducted using experimental reactivity data or data calculated classically using DFT. Subsequently, the trained model is used in the inference stage b) to predict new molecular reactivities. Figure taken exactly from [4]. Reproduced with permission.*

In this approach, a molecule or series of molecules with chemical similarity is explored using a molecular fragment relevant to the problem to reduce the complexity of the problem. Once the fragment of interest has been defined, suitable embedding methods and active space selection are performed to obtain an effective Hamiltonian that describes the fragment and its entanglement with the rest of the molecule (and eventually the rest of the environment around the molecule e.g. water). The effective Hamiltonian can be used to obtain insights

into the dynamics of the system, from which the input features for the machine learning model may be derived. In our case, we select expectation values of some observables, measured at the certain time-evolved states of our system, called ‘*quantum fingerprints*’. To perform this task using quantum computers, the Hamiltonian dynamics of the system will be simulated as shown in Section II. Finally, the machine learning model will be trained to predict an interesting objective by using the training (and testing) dataset of molecules with experimental measurement values.

III. METHODOLOGY

Following the methodology outlined in [4], most of the details for the use case (Subsection III A) were adapted from this reference, with the exception of the molecular dataset. Extensions to the original approach are detailed in the Subsections from III B to III E.

A. Use case details

The dataset includes a series of targeted covalent drugs with the sulfonyl fluoride (SO_2F) reactive group (known as a ‘warhead’), which is also the fragment of interest. Raw data contain 276 molecules with single structural confinement. In this work, we select 8 molecules from the dataset of the original paper [4] while the remaining molecules were taken from PubChem database. The split for cross-validation was 85% for the training dataset and 15% for the test dataset. The chemical structure of 3 representative molecules is shown in Figure 2.

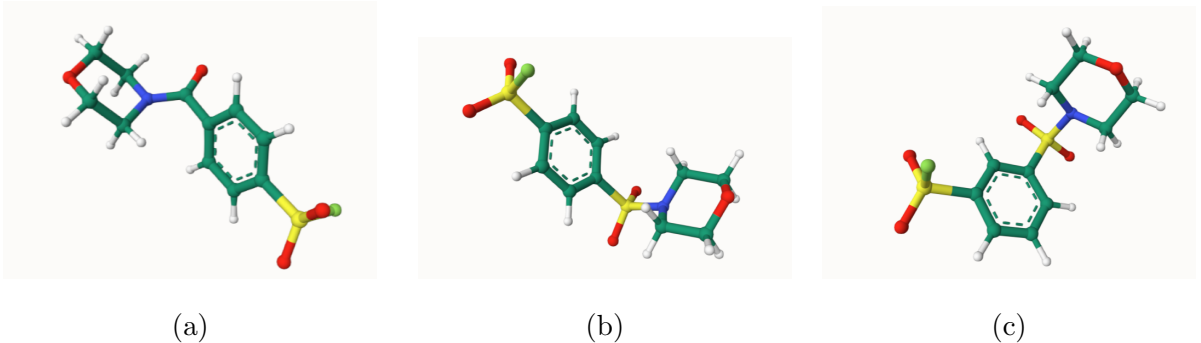


FIG. 2: 2D diagram structures of 3 exemplary molecules from the dataset. Respectively a) 4-(Morpholine-4-carbonyl)benzene-1-sulfonyl fluoride, b) 4-(Morpholine-4-sulfonyl)benzene-1-sulfonyl fluoride, c) 3-Morpholin-4-ylsulfonylbenzenesulfonyl fluoride.

Ground truth reactivities were simulated with DFT as a linear regression between the measured rate constant (or half-life) and the LUMO energy [4, 16].

To create the electronic structure Hamiltonians, LUMO energies calculated with B3LYP-D3 functional on the $6-31+G^{**}$ basis set were used. The rationale behind not using directly the experimental values is to give a proof of concept for reproducing values coming from quantum mechanical calculations on classical computers. The embedding is done using Density Matrix Embedding Theory (DMET) along with the active space reduction described in [4]. The details of experiments preparation for quantum computers are described in Sections B and C. The initial state of the simulated fragments will be Hartree-Fock initial state, since for this dataset and this problem it yields the best ML model performance in comparison to other initial states [4]. As the observable yielding the quantum fingerprint, the temporal observable will be taken, which is defined as:

$$F(t) = \sum_{r,s} h_{rs}^{eff} \rho_{rs}(t)$$

Where $\rho_{rs}(t) = \langle \psi(t) | \hat{a}_s^\dagger \hat{a}_r | \psi(t) \rangle$ is the one-body density matrix of the embedded fragment, where r and s are the localized orbitals in the chosen fragment and the h_{rs}^{eff} are the effective one-electron integrals from the embedded effective Hamiltonian. This observable yields a quadratic number of terms, so a quadratic number of Pauli measurement operators from the active space size. Based on this observable expectation value, the feature vector will be created as the sampled observable trajectory within the time range $t \in [0, 14] t/t_h$ with the sampling interval $\Delta t = 0.5 t/t_h$. Finally, the objective of the machine learning model is the

prediction of the molecule reactivity, for which the ground truth will be reactivity simulated with classical methods as described in the previous section. As the model architecture, the Partial Least Squares Regression (PLS) will be used.

B. Quantum experiments pipeline

This section describes the procedure of obtaining quantum fingerprints in the use case, starting with the qubit-mapped Hamiltonian and the initial Hartree-Fock state and ending with the input feature vector for the reactivity prediction model.

As mentioned in Section A the initial state, the Hamiltonian, and the observables in the second quantized fermionic form need to be qubit mapped with the Jordan-Wigner transform. For the scope of this paper, three generic qubit mapping methods were tested and compared and Jordan-Wigner was chosen since it yields the shallowest circuits for the smallest active spaces. Detailed results are in the Appendices D and F. More advanced methods are pointed out in the Discussion Section VI.

All simulations will be run with the 1st order Product Formula decomposition with 1 Trotter step, since the main goal is to get the Hamiltonian simulation method with shallowest circuits feasible to run on real QPUs for larger active space sizes, no matter the algorithmic approximation done by the method. The idea is to reduce the circuits yielded by the method until it is feasible to run on a real QPU. That allows us to evaluate the accuracy of the predictive models with the current QPUs capability. Based on that, further work on increasing the accuracy of the solution (either by using further circuit reduction methods or running experiments on QPUs of higher fidelities) can be done. Also, circuit depths obtained for this simplest case may be easily extrapolated on more trotter steps and higher-order PFs. That will be helpful for resource estimation of accurate approximations. The accuracy of our approximation will be assessed in Appendix E A by evaluating the predictive model accuracy with the Root Mean Squared Error (RMSE) metric. For the ground truth values of the predicted reactivity, both for model training and inference, classically calculated reactivity as described in the Subsection above will be used.

So far only the original paper setup has been presented. This paper extends previous work with the enhancements allowing to run active space sizes larger than the smallest one (2e, 4so) on real QPUs. Those improvements can be applied on four levels, reflecting also

sequentially how they are executed during real-time evolution simulation routine:

1. problem algorithmic preparation - initial state, Hamiltonian and observables preparation, qubit mapping, and product formulas decomposition
2. simulation circuit synthesis - circuit construction from the initial state and Hamiltonian terms exponentiation
3. ISA circuit preparation - synthesized circuit transpilation on the desired backend
4. quantum error mitigation and suppression - specification of the error mitigation and suppression protocols and running the experiments using these protocols

On each level, improvements may be generic (problem-agnostic) and problem-aware, leveraging information about the problem. Our propositions of improvement are as follows:

1. problem algorithmic preparation - truncation of Hamiltonian terms (described in Appendix E A)
2. simulation circuit synthesis - Clifford Decomposition and Transformation (CDAT)(Appendix E C)
3. transpilation (ISA circuit preparation) - transpilation techniques particularly focused on gates cancellation, effective assigning out virtual qubits to physical ones generating the least amount of 2-qubit gates (subsection III C.)
4. error mitigation and suppression - build-in protocols in Qiskit (subsection III E)

On top of that, Haiqu middleware is incorporated (Subsection III D) and it covers levels 2, 3, and 4. The techniques from the first two levels are described in the Appendices, while the details of the last two levels' details are provided in this subsection. A graphical composition of the techniques used can be found in Figure 3.

The circuit depths obtained after straightforward exponentiation of the qubit mapped Hamiltonians to the *Clifford + R_z* set of gates, for a range of active spaces, will be the point of reference for circuit reductions in the presented methods.

The optimization starts from the qubit-mapped Hamiltonian terms. Terms with small coefficients cannot significantly influence the measured observable expectation value, since only a narrow initial range for the time evolution is sampled ($t \in [0, 14] t/t_h$).

Effective qubit Hamiltonians obtained from the used dataset for checked ranges of active space sizes (2e,4so)-(22e, 44so) have coefficients of terms spanning orders of magnitudes

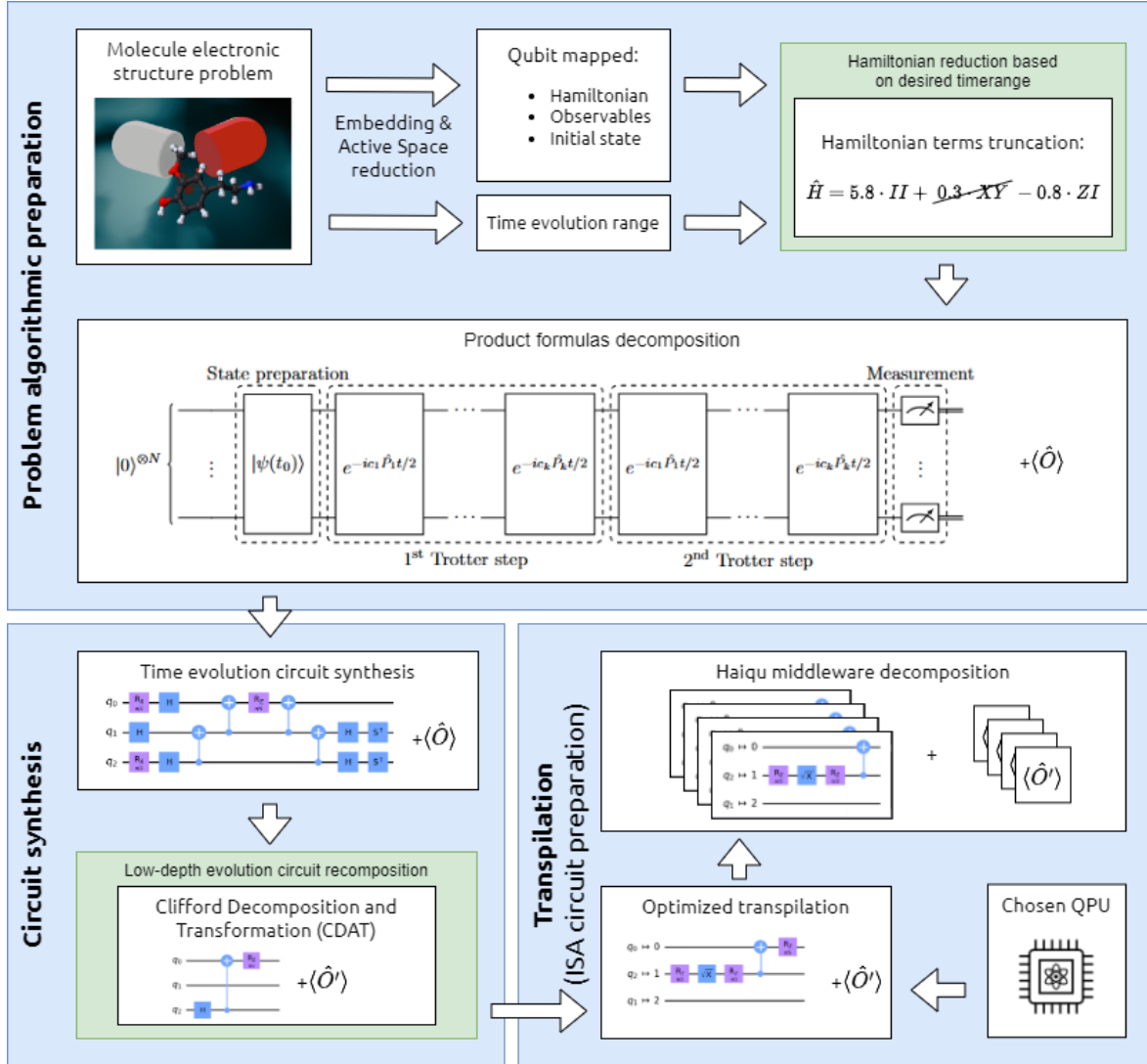


FIG. 3: Flowchart of the optimized real-time evolution simulation execution on quantum computers consisting of three parts - Problem algorithm preparation, Circuit synthesis, and Transpilation. Blue rectangles mark the steps of the time-evolution circuit preparation.

($10^{-1} - 10^{-7}$) that allow to safely exclude most of the terms for the simulation. A representative example for (6e,12so) is shown in the Appendix G. The exact truncation algorithm that was used in this paper is based on the maximum expectation value's change $\epsilon_{d\langle \hat{A} \rangle}$ induced by removing the terms out of the Hamiltonian. It is introduced in Figure 16.

The next step is the optimization on the circuit synthesis level. There, the CDAT transformation is applied to further reduce the circuit depth, by effectively getting rid of the majority of the Clifford gates. Results for simulation circuit reduction for the combination of CDAT and truncation based on the observable error for max. range of simulation time

are presented in the Results Section VB.

C. Instruction Set Architecture (ISA) circuit preparation

For QPU transpilation, Qiskit’s transpiler was used, particularly the preset pass manager from Qiskit 1.2 with the *optimization_level=2* (transpilation option enabling: number of swap gates minimization, canceling inverse gates, reducing 1-qubit gates and applying layout/routing heuristics optimized with greater search depth and trials of optimization function, than lower optimization levels), ‘sabre’ method for both layout and routing options chosen.

For comparison we also tried the algorithm presented in [32], called *Rustiq*, in order to generate the evolution circuit, before mapping it to the device. This algorithm solves the problem of implementing a given sequence of multi-qubit Pauli rotations using only single- and two-qubit gates. It proceeds by scoring each and every possible single-CNOT piece of the circuit (called ‘chunks’) by conjugating all the remaining Pauli rotations through it. The score of a chunk will roughly correspond to how much progress was made in reducing the weights of all remaining rotations, with an emphasis on the first rotations in the list. The algorithm greedily builds a circuit by picking the highest scoring chunk, conjugating all rotations through it, injecting weight one rotations as single-qubit gate, and carrying on. By considering the full sequence of rotations when scoring each chunk, this algorithm is able to exploit global symmetries of the input to greatly reduce the overall gate count and depth. This approach can improve the depth of Hamiltonian simulation circuits by a factor of 10 on standard chemistry benchmarks [32].

D. Middleware application

For real QPU experiments, the middleware from Haiqu was used. Haiqu middleware targets each aspect of the quantum computing workflow to streamline it: analysis of the circuits’ properties, particularly in relation to the intended hardware, custom compilation packages, error mitigation (EM), and circuit execution and post-processing. The system provides both improved versions of some of the individual components as well as the capacity to orchestrate these and combine them with the Optimized Execution circuit execution

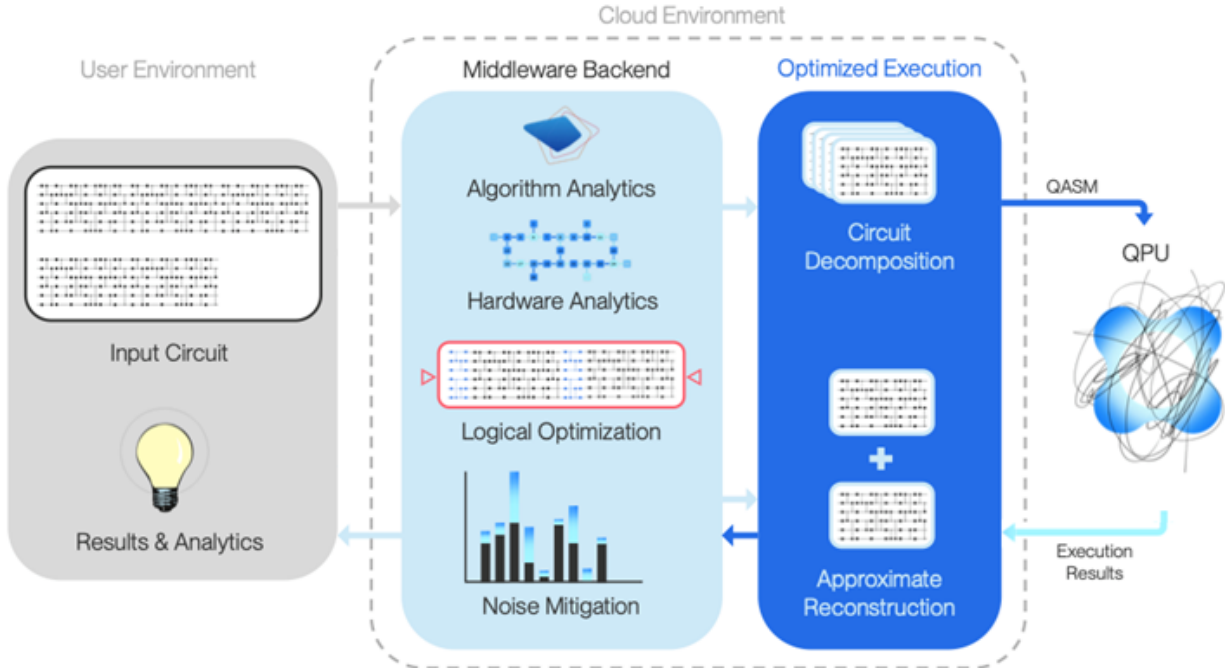


FIG. 4: *Workflow of the Optimized Execution strategy developed by Haiqu. It is a strategy for executing multiple modified algorithm sub-blocks in a sequential or parallel fashion and then reconstructing the final or intermediate quantum state. It is distinct from circuit partitioning and synthesis strategies and combines aspects of standard compilation and error mitigation techniques.*

strategy.

The proprietary Optimized Execution (OE) strategy is based on executing, in a sequential or parallel fashion, multiple modified algorithm sub-blocks and subsequently reconstructing the final or intermediate quantum state. It superficially resembles, but is distinct from, circuit partitioning [33] and synthesis strategies e.g. [34], and combines aspects of both standard compilation and error mitigation techniques.

Each individually executed sub-block is ensured to fit the practical performance constraints of the QPU, minimizing the accumulated errors, and allowing to reproduce the results of running a quantum algorithm whose length would naively place it beyond the coherence time of the device. The high-level flow diagram is shown at Figure 4.

As such an execution strategy is not directly a compilation approach nor a noise mitigation technique, it can be combined with other techniques to further improve the results.

E. Error mitigation methods

Using error mitigation and suppression is a go-to, both in terms of how common it is for the real backend experiments in other publications and current accessibility and usage convenience in quantum SDK e.g. Qiskit. In this paper only the methods with small overheads will be used, so that they can be applicable with the middleware (that multiplies the overhead further), and also estimations of a few time points, instead of a single one, would be possible in a reasonable time frame.

For this reason, QPU experiments will be run with readout error mitigation (T-REx) plus Pauli Twirling[35] from the quantum error mitigation side and Dynamical Decoupling [36] due to circuit sparsity from the quantum error suppression site. With a sufficient number of shots, those three methods combined decrease common types of errors and should yield results in shallow confidence intervals allowing to potentially further improve the results with Zero Noise Extrapolation (ZNE) [37].

IV. COMPUTATIONAL DETAILS

For the software the classical computing work (mainly quantum chemistry simulations) was done in Python with PySCF [38], Vayesta [39] and Qiskit (particularly Qiskit Nature) packages [40, 41]. All code and simulations were run locally on a laptop with Intel i7 9th gen CPU 2.6GHz, NVIDIA Quadro T1000, and 32GB of RAM. Quantum computing parts of this paper were set up and run using native Qiskit 1.2 and its extensions in Python, both for reference, ideal simulations, and real backend experiments. Ideal simulations were run on Qiskit Aer simulator with GPU as a backend. All QPU estimations were run on IBM’s superconducting qubits backends with the newest IBM’s Heron R2 architecture [42] in the batch mode. Each time point was run during the same calibration cycle with a total number of 8192 shots, 64 Pauli twirls (128 shots per twirl), 16 T-REx randomizations (100 shots per randomization), and Dynamical Decoupling with ‘ $X_p X_m$ ’ type of sequence. For the Haiqu middleware runs, all details are provided in Appendix H.

V. RESULTS

A. Hamiltonian terms truncation results

To graphically show the influence of removing terms from the Hamiltonian in Figure 5, the energy trajectories from different numbers of terms left in the Hamiltonian were plotted for 8 spin-orbitals case of an exemplary molecule. The trajectories were calculated on a noiseless simulator, and only terms of the highest absolute values of coefficients were left per each trajectory. The mean absolute error (MAE) between each trajectory and trajectory based on the full Hamiltonian was shown in Figure 6. For reference, for the observable error limit $\epsilon_{d(\hat{A})} = 1\%$ for the max. time 100 (a.u.), according to the presented truncation algorithm (Appendix V B) 42.45% of terms should be left, and around 40% we see the value of MAE close to 0.2, which is roughly 1% of the smallest absolute values of the energy.

The final objective of our use case is not the trajectories themselves, but the reactivities of drugs predicted with ML model based on them. In Figure 7, the prediction of reactivities was evaluated on the ML model and dataset as described in the Methodology Section. Per each active space, the PLS model was trained for a number of components yielding the best

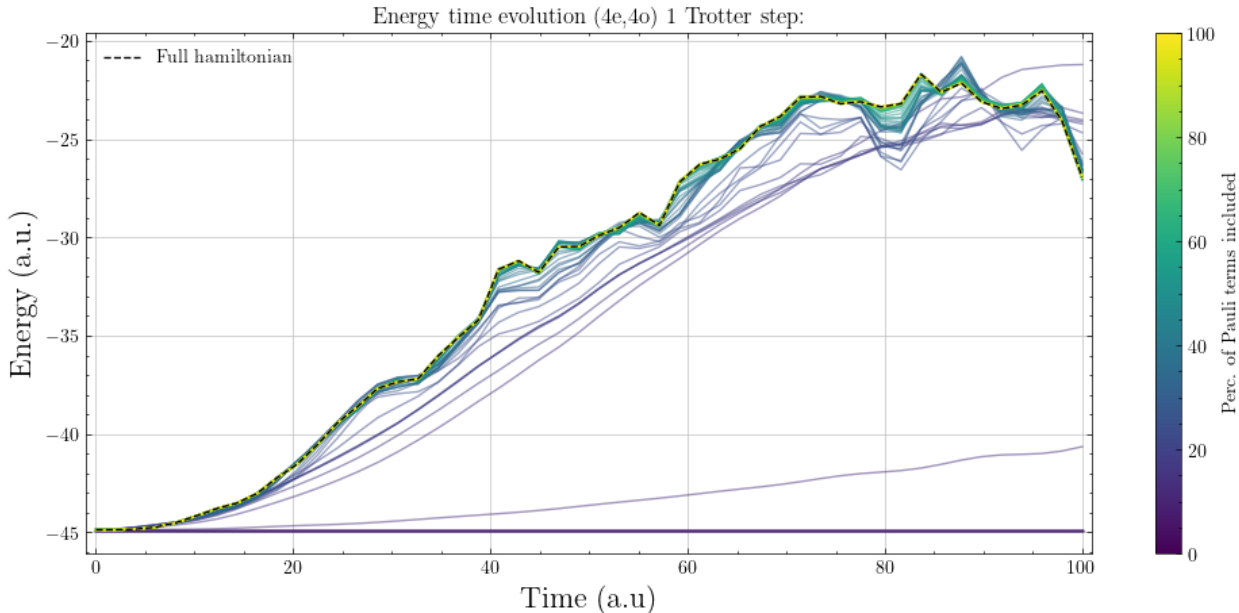


FIG. 5: Energy trajectories simulated without any noise and without sampling over a range of terms left in the Hamiltonian for an exemplary molecule of the active space with 8 spin-orbitals.

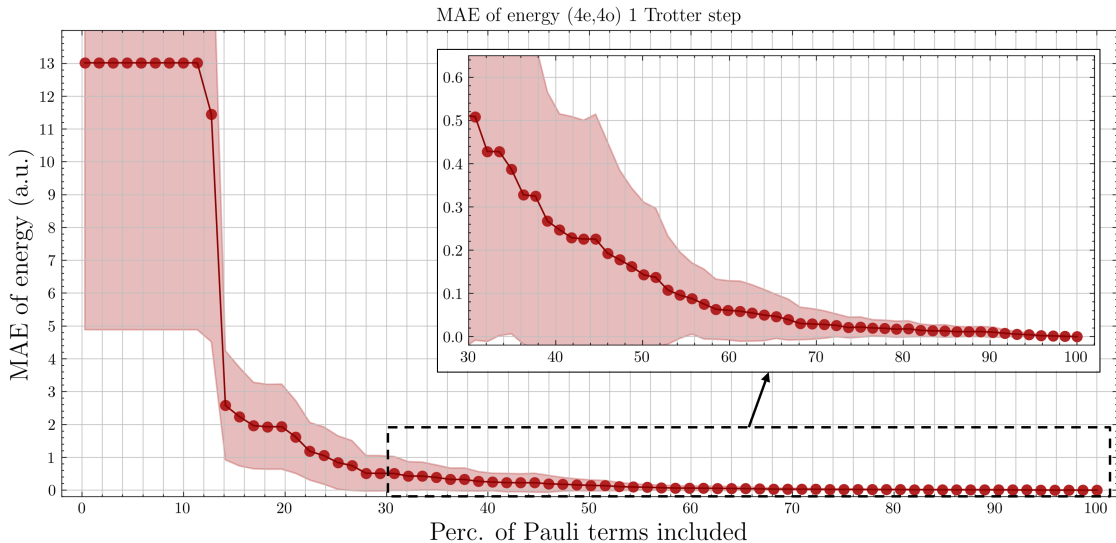


FIG. 6: Mean absolute error (MAE) between trajectories simulated over a range of terms left in the Hamiltonian and the reference trajectory based on full Hamiltonian. The Hamiltonian and the initial state were taken for an exemplary molecule of active space 8 spin-orbitals, same as in Figure 5. The dots illustrate the mean and the semi-transparent area standard deviation.

evaluation scores for a given active space size. Training and testing was done with 5-fold cross-validation. The evaluation was performed for each active space over input trajectories simulated with truncated Hamiltonians from 1% of terms left to 100% of terms left (full Hamiltonian). Each data point per active space per percentage of Hamiltonian terms left denotes a single training and testing model from scratch.

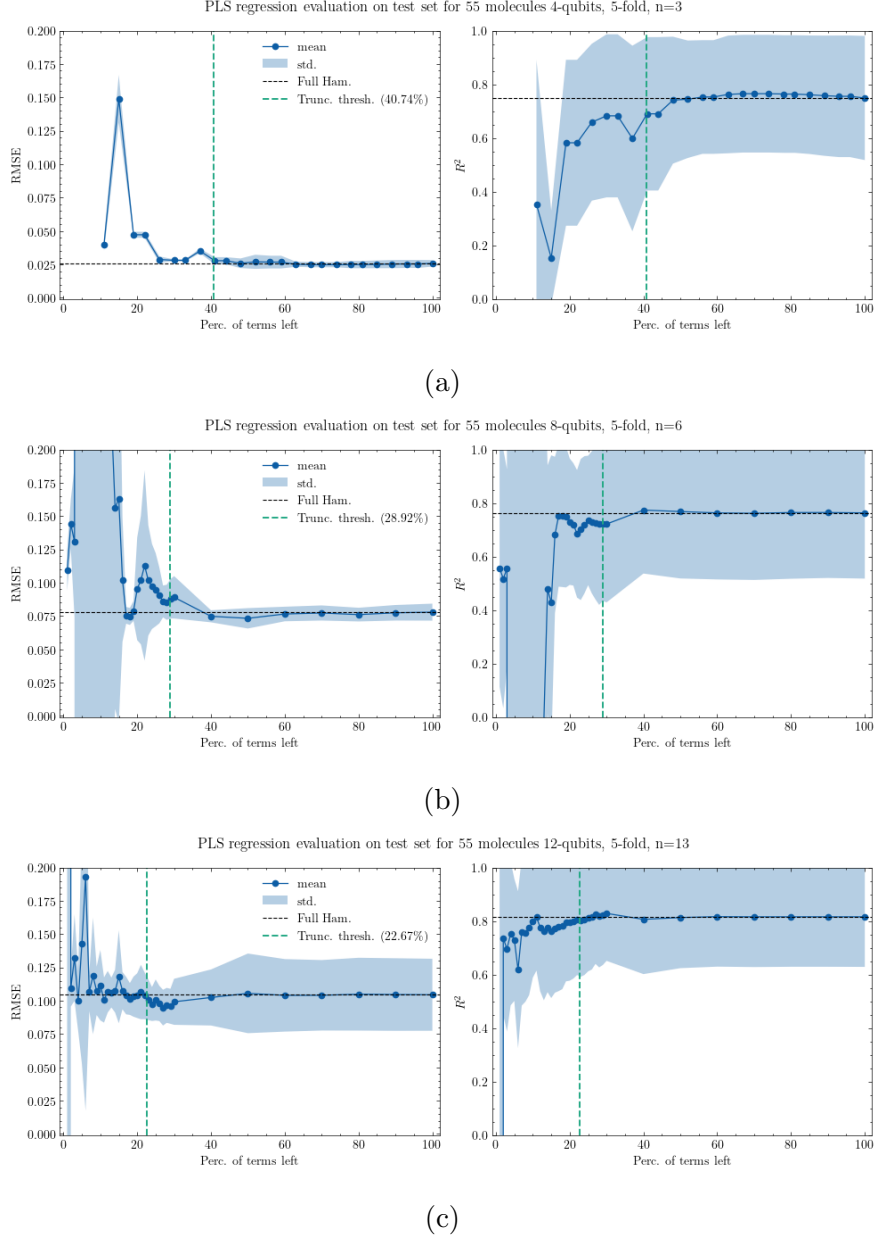


FIG. 7: *Evaluation metrics comparison over a) (2e,4so), b) (4e,8so) and c) (6e,12so) active spaces for PLS. The results show the mean of evaluation metrics: the Root Mean Squared Error (RMSE), and explained variance (R^2) from test sets. Each test set contained 55 molecules. PLS components are listed in the titles as ‘n’. The horizontal line denotes scores for the full Hamiltonian (100% of terms). For reference, the truncation threshold for $\epsilon_{d(\hat{A})} = 1\%$ for the max. time 14 (a.u.) time based on the molecule from Result Section VB was drawn vertically.*

For strong truncation with small percentages of terms left, there is an expected decrease in performance, both for RSME and R^2 . After considering the percentage threshold for

$\epsilon_{d(\langle \hat{A} \rangle)} = 1\%$ taken from reference molecule from the Result Section V B, all truncations with more terms allow to maintain similar performance as for full Hamiltonian. That is also expected since the terms included above that threshold have small coefficients inducing small changes to trajectory. Interestingly, similar performance might be observed also for some data points below the reference threshold. This indicates, that even if trajectories from truncated Hamiltonian may differ above 1% for far time regimes in comparison to full Hamiltonian’s ones, this does not influence the PLS evaluation metric significantly. Thanks to that, reactivity prediction might be done on even shallower circuits, without a drop in its performance.

B. Circuits reduction results

A combination of Hamiltonian terms truncation reduction (for observable error limit $\epsilon_{d(\langle \hat{A} \rangle)} = 1\%$ for the max. time 14 (a.u.)) with CDAT or Rustiq reduces the circuit depths by slightly above one order of magnitude as shown in Figure 8 on an exemplary molecule. The same results up to 16 qubits numerically were shown in Table I along with the circuit depths for real QPU after transpilation to IBM’s Heron R2 architecture. Circuits were transpiled with Qiskit 1.2 [40] generic pass manager with *optimization_level=2* on all-to-all connectivity with *Clifford + R_z* set of gates (Figure 8 and left part of Table I) and IBM Heron R2 architecture (right part of Table I). The depths are the best results from 50 transpilation trials. All this data was plotted in the abstract figure. The displayed methods are ‘Default’ denoting full Hamiltonian-based circuit (‘No reduction’), ‘Truncation’ - truncated Hamiltonian-based circuit (‘Reduction level 1’), ‘Truncation+CDAT’ - truncated Hamiltonian-based circuit with Clifford Decomposition and Transformation (CDAT) applied (‘Reduction level 2’), and ‘Truncation+Rustiq’ - truncated Hamiltonian-based circuit with Rustiq transpiler’s circuit synthesis applied (‘Reduction level 3’).

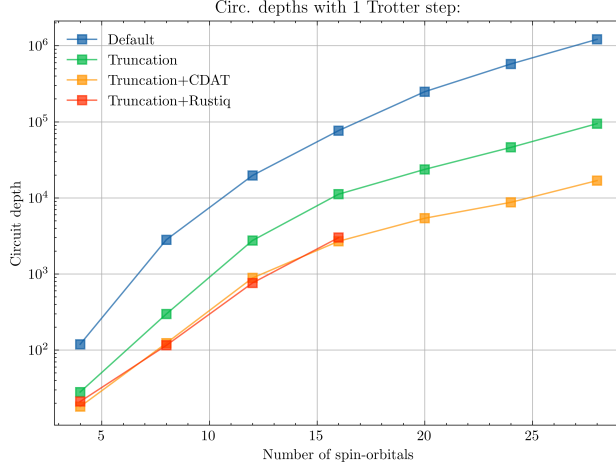


FIG. 8: Depths of the quantum circuits for 1 Trotter step for time evolution simulation of qubit mapped effective fragment Hamiltonian for an exemplary molecule through active space size with Jordan-Wigner qubit mapping and the Hartree-Fock initial state.

	Active Space Size			
	(2e/4so)	(4e/8so)	(6e/12so)	(8e/16so)
Default	119	2812	19669	76523
Truncation	28	297	2748	11169
(reduction)	(4.3x)	(9.5x)	(7.2x)	(6.9x)
CDAT	18	123	884	2688
(reduction)	(6.6x)	(22.9x)	(22.3x)	(28.5x)
Rustiq	21	115	760	2999
(reduction)	(5.7x)	(24.5x)	(25.9x)	(25.5x)

	Active Space Size			
	(2e/4so)	(4e/8so)	(6e/12so)	(8e/16so)
Default	293	7015	49388	195611
Truncation	102	823	8104	33356
(reduction)	(2.9x)	(8.5x)	(6.1x)	(5.9x)
CDAT	39	585	3916	12650
(reduction)	(7.5x)	(12.0x)	(12.6x)	(15.5x)
Rustiq	57	677	6101	27140
(reduction)	(5.2x)	(10.4x)	(8.1x)	(7.2x)

(a) Quantum simulators circuits for all-to-all qubits connectivity for Clifford+ R_z gates

(b) ISA circuits on IBM's Heron R2 architecture

TABLE I: Circuit depths for different circuit reduction options on an exemplary molecule simulation circuit for 1 Trotter step. Truncation circuits were generated for limit $\epsilon_{d(\langle \hat{A} \rangle)} = 1\%$ for the max. time 14 (a.u.)

C. Real QPU results

Reference results from the runs with generic error mitigation (as described in the Methodology Section) and with Haiqu middleware, are shown in Figure 9. Circuits were prepared with constrained truncation for observable error limit $\epsilon_{d(\langle \hat{A} \rangle)} = 0.5\%$ for the max. time 14

(a.u.) and after CDAT.

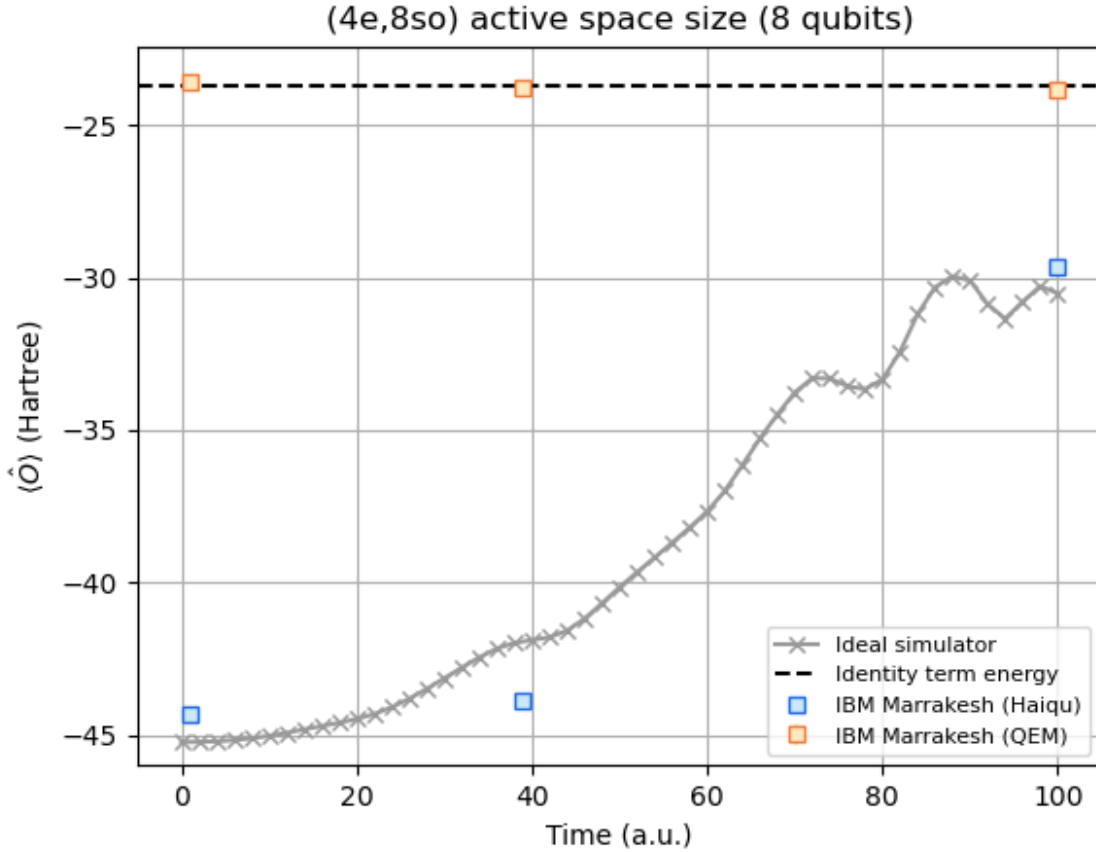


FIG. 9: Results comparison for the run on the real hardware with Qiskit build-in error mitigation (QEM) and Haiqu middleware (Haiqu).

VI. DISCUSSION

The approach proposed in this work might be further extended with other methods, and those should be tested next to enable even larger active spaces runs. The emphasis could be put on circuit decompositions or in general techniques decreasing the circuit depths at the cost of increased overheads e.g. a number of experiments on real QPUs, such as operator backpropagation [41], circuit knitting [43], repeated qubit tapering, or methods including post-processing [7, 44].

Generic qubit mappings that were applied may not be the best starting point, the circuit depth may be reduced even further by applying more efficient methods [45]. Particularly

interesting are the ones considering qubit connectivity at real backends [46], [47].

For real backend runs, more extensive quantum error mitigation could be used giving more accurate results, however, that would add significant overhead also to experiments with Haiqu middleware.

ML model evaluation from the truncation level showed larger significance of terms with the largest absolute values of coefficients, than small ones, for predictive models not only for the trajectory accuracy. Also, PLS demonstrates some error robustness, keeping relatively the same performance for truncation slightly below the pessimistic bound based on a maximum error in trajectory in far ranges.

From the ML perspective, the PLS models evaluation for the trade-off between prediction accuracy and truncation level shows similar performance for trajectories simulated with truncated Hamiltonian below $\epsilon_{d(\hat{A})} = 1\%$ bounds based on trajectory accuracy over 3 active spaces. This results potentially enables even further reduction of quantum circuits depth through replacing current worst-case-scenario bounded truncation based on trajectories accuracy with truncation based on the predictive models performance. That approach is readily available, seems scalable towards larger active spaces, based on results could cut down Hamiltonian terms by another few percentage points depending on active space, and could be evaluated for circuit reduction prior to extending the pipeline with novel methods.

VII. CONCLUSIONS

This work demonstrates significant advancements in reducing the circuit depth of quantum chemistry problems that can be run on today’s quantum systems. By applying hardware-efficient approaches and optimized algorithms, we achieved up to a 28.5-fold reduction on an emulated backend. Moreover, we achieved a 15.5-fold reduction in circuit depths for experiments run on IBMQ’s Heron quantum system, with an approach scalable towards 24+ qubits.

Specifically, we applied several circuit reduction techniques to enable Hamiltonian simulation of larger active spaces for covalent inhibitor reactivity prediction:

1. Hamiltonian terms truncation based on observable error limits
2. Clifford Decomposition and Transformation (CDAT)
3. Optimized transpilation techniques

By combining these methods and applying the quantum error mitigation and suppression

we managed to run, with the support of Haiqu middleware, simulations on 8-qubit circuits on real quantum hardware, which represents an increase from previous 4-qubit demonstrations. More importantly, the methods used here systematically reduce the circuits for Hamiltonian simulation for more than an order of magnitude for the tested range of active spaces between (2e, 4so) and (14e, 28so). This showcases the proposed approach as a scalable tool to help run the Hamiltonian simulation on more qubits than shown in this work, by further extending the circuit reduction approach with other methods and quantum hardware error tolerance improvement. Our results show that even with aggressive circuit reduction and approximations, we can still obtain reasonable predictions for molecular reactivity using the Quantum-Centric Data-Driven R&D (QDDRD) framework.

The overarching impact of this work is that it highlights promising methods that allow researchers to explore the dynamics of commercially relevant chemistry problems on real quantum hardware via Hamiltonian simulation. As quantum hardware continues to improve, these techniques can be scaled to enable simulation of even larger molecular systems.

Future work should focus on further optimizing these circuit reduction techniques, exploring more efficient qubit mapping methods, and investigating how to balance algorithmic approximations with prediction accuracy as system sizes increase. Additionally, as quantum hardware improves, reassessing the trade-offs between circuit depth reduction and simulation accuracy will be crucial for maximizing the utility of quantum computers for chemistry applications.

-
- [1] R. P. Feynman, Simulating physics with computers, *International Journal of Theoretical Physics* **21**, 467 (1982).
- [2] Y. Alexeev, M. Amsler, M. A. Barroca, S. Bassini, T. Battelle, D. Camps, D. Casanova, Y. J. Choi, F. T. Chong, C. Chung, C. Codella, A. D. Córcoles, J. Cruise, A. D. Meglio, I. Duran, T. Eckl, S. Economou, S. Eidenbenz, B. Elmegreen, C. Fare, I. Faro, C. S. Fernández, R. N. B. Ferreira, K. Fuji, B. Fuller, L. Gagliardi, G. Galli, J. R. Glick, I. Gobbi, P. Gokhale, S. de la Puente Gonzalez, J. Greiner, B. Gropp, M. Grossi, E. Gull, B. Healy, M. R. Hermes, B. Huang, T. S. Humble, N. Ito, A. F. Izmaylov, A. Javadi-Abhari, D. Jennewein, S. Jha, L. Jiang, B. Jones, W. A. de Jong, P. Jurcevic, W. Kirby, S. Kister, M. Kitagawa, J. Klassen, K. Klymko, K. Koh, M. Kondo, D. M. Kurkcuoglu, K. Kurowski, T. Laino, R. Landfield, M. Leininger, V. Leyton-Ortega, A. Li, M. Lin, J. Liu, N. Lorente, A. Luckow, S. Martiel, F. Martin-Fernandez, M. Martonosi, C. Marvinnay, A. C. Medina, D. Merten, A. Mezzacapo, K. Michielsen, A. Mitra, T. Mittal, K. Moon, J. Moore, S. Mostame, M. Motta, Y.-H. Na, Y. Nam, P. Narang, Y. ya Ohnishi, D. Ottaviani, M. Otten, S. Pakin, V. R. Pascuzzi, E. Pednault, T. Piontek, J. Pitera, P. Rall, G. S. Ravi, N. Robertson, M. A. C. Rossi, P. Rydlichowski, H. Ryu, G. Samsonidze, M. Sato, N. Saurabh, V. Sharma, K. Sharma, S. Shin, G. Slessman, M. Steiner, I. Sitdikov, I.-S. Suh, E. D. Switzer, W. Tang, J. Thompson, S. Todo, M. C. Tran, D. Trenev, C. Trott, H.-H. Tseng, N. M. Tubman, E. Tureci, D. G. Valiñas, S. Vallecorsa, C. Wever, K. Wojciechowski, X. Wu, S. Yoo, N. Yoshioka, V. W. zhe Yu, S. Yunoki, S. Zhuk, and D. Zubarev, Quantum-centric supercomputing for materials science: A perspective on challenges and future directions, *Future Generation Computer Systems* **160**, 666 (2024).
- [3] G. K.-L. Chan, Quantum chemistry, classical heuristics, and quantum advantage (2024).
- [4] T. W. A. Montgomery, P. Pogány, A. Purdy, M. Harris, M. Kowalik, A. Ferraro, H. Hasan, D. V. S. Green, and S. Genway, Data-driven reactivity prediction of targeted covalent inhibitors using computed quantum features for drug discovery (2023).
- [5] A. Shajan, D. Kaliakin, A. Mitra, J. R. Moreno, Z. Li, M. Motta, C. Johnson, A. A. Saki, S. Das, I. Sitdikov, A. Mezzacapo, and K. M. M. Jr, Towards quantum-centric simulations of extended molecules: sample-based quantum diagonalization enhanced with density matrix embedding theory (2024).

- [6] K. Kanno, M. Kohda, R. Imai, S. Koh, K. Mitarai, W. Mizukami, and Y. O. Nakagawa, Quantum-selected configuration interaction: classical diagonalization of hamiltonians in subspaces selected by quantum computers (2023).
- [7] J. Robledo-Moreno, M. Motta, H. Haas, A. Javadi-Abhari, P. Jurcevic, W. Kirby, S. Martiel, K. Sharma, S. Sharma, T. Shirakawa, I. Sitdikov, R.-Y. Sun, K. J. Sung, M. Takita, M. C. Tran, S. Yunoki, and A. Mezzacapo, Chemistry beyond exact solutions on a quantum-centric supercomputer (2024).
- [8] S. Barison, J. R. Moreno, and M. Motta, Quantum-centric computation of molecular excited states with extended sample-based quantum diagonalization (2024).
- [9] D. W. Berry, D. Motlagh, G. Pantaleoni, and N. Wiebe, Doubling the efficiency of hamiltonian simulation via generalized quantum signal processing, *Physical Review A* **110**, 10.1103/physreva.110.012612 (2024).
- [10] J. Ostmeyer, Optimised trotter decompositions for classical and quantum computing, *Journal of Physics A: Mathematical and Theoretical* **56**, 285303 (2023).
- [11] P. Mukhopadhyay, N. Wiebe, and H. T. Zhang, Synthesizing efficient circuits for hamiltonian simulation, *npj Quantum Information* **9**, 31 (2023).
- [12] A. W. Harrow and A. Lowe, Optimal quantum circuit cuts with application to clustered hamiltonian simulation (2024).
- [13] G. Lee, D. Lee, and J. Huh, Sampling error analysis in quantum krylov subspace diagonalization, *Quantum* **8**, 1477 (2024).
- [14] W. van Dam, H. Liu, G. H. Low, A. Paetznick, A. Paz, M. Silva, A. Sundaram, K. Svore, and M. Troyer, End-to-end quantum simulation of a chemical system (2024).
- [15] H. Liao, D. S. Wang, I. Sitdikov, C. Salcedo, A. Seif, and Z. K. Mineev, Machine learning for practical quantum error mitigation (2023).
- [16] K. E. Gilbert, A. Vuorinen, A. Aatkar, P. Pogány, J. Pettinger, E. K. Grant, J. M. Kirkpatrick, K. Rittinger, D. House, G. A. Burley, and J. T. Bush, Profiling sulfur(vi) fluorides as reactive functionalities for chemical biology tools and expansion of the ligandable proteome, *ACS Chemical Biology* **18**, 285 (2023), doi: 10.1021/acscchembio.2c00633.
- [17] R. P. Bhole, G. O. Joshi, H. S. Kapare, R. V. Chikhale, and S. Chaudhari, Covalent drug – an emerging framework for targeted drug development, *Results in Chemistry* **8**, 101615 (2024).
- [18] L. Boike, N. J. Henning, and D. K. Nomura, Advances in covalent drug discovery, *Nature*

- Reviews Drug Discovery **21**, 881 (2022).
- [19] J. Singh, The ascension of targeted covalent inhibitors, *Journal of Medicinal Chemistry* **65**, 5886 (2022), doi: 10.1021/acs.jmedchem.1c02134.
- [20] K. McAulay, A. Bilsland, and M. Bon, Reactivity of covalent fragments and their role in fragment based drug discovery, *Pharmaceuticals* **15**, 10.3390/ph15111366 (2022).
- [21] R. Lonsdale, J. Burgess, N. Colclough, N. L. Davies, E. M. Lenz, A. L. Orton, and R. A. Ward, Expanding the armory: Predicting and tuning covalent warhead reactivity, *Journal of Chemical Information and Modeling* **57**, 3124 (2017), doi: 10.1021/acs.jcim.7b00553.
- [22] S. Lloyd, Universal quantum simulators, *Science* **273**, 1073 (1996).
- [23] D. W. Berry and A. M. Childs, Black-box hamiltonian simulation and unitary implementation, *Quant. Inf. Comput.* **12**, 29 (2012).
- [24] D. W. Berry, A. M. Childs, R. Cleve, R. Kothari, and R. D. Somma, Exponential improvement in precision for simulating sparse hamiltonians, in *Proceedings of the Forty-Sixth Annual ACM Symposium on Theory of Computing* (Association for Computing Machinery, 2014) pp. 283–292.
- [25] D. W. Berry, A. M. Childs, R. Cleve, R. Kothari, and R. D. Somma, Simulating hamiltonian dynamics with a truncated taylor series, *Phys. Rev. Lett.* **114**, 90502 (2015).
- [26] G. H. Low and I. L. Chuang, Optimal hamiltonian simulation by quantum signal processing, *Physical Review Letters* **118**, 10.1103/physrevlett.118.010501 (2017).
- [27] A. M. Childs, D. Maslov, Y. Nam, N. J. Ross, and Y. Su, Toward the first quantum simulation with quantum speedup, *Proceedings of the National Academy of Sciences* **115**, 9456 (2018).
- [28] M. Reiher, N. Wiebe, K. M. Svore, D. Wecker, and M. Troyer, Elucidating reaction mechanisms on quantum computers, *Proceedings of the National Academy of Sciences* **114**, 7555 (2017).
- [29] T. P. Gujarati, M. Motta, T. N. Friedhoff, J. E. Rice, N. Nguyen, P. K. Barkoutsos, R. J. Thompson, T. Smith, M. Kagele, M. Brei, B. A. Jones, and K. Williams, Quantum computation of reactions on surfaces using local embedding, *npj Quantum Information* **9**, 88 (2023).
- [30] S. Bravyi, J. M. Gambetta, A. Mezzacapo, and K. Temme, Tapering off qubits to simulate fermionic hamiltonians (2017).
- [31] K. Setia, R. Chen, J. E. Rice, A. Mezzacapo, M. Pistoia, and J. D. Whitfield, Reducing qubit requirements for quantum simulations using molecular point group symmetries, *Journal of Chemical Theory and Computation* **16**, 6091 (2020).

- [32] T. G. de Brugière and S. Martiel, Faster and shorter synthesis of hamiltonian simulation circuits (2024).
- [33] K. Mitarai and K. Fujii, Constructing a virtual two-qubit gate by sampling single-qubit operations, *New Journal of Physics* **23**, 23021 (2021).
- [34] K. N. Patel, I. L. Markov, and J. P. Hayes, Efficient synthesis of linear reversible circuits (2003).
- [35] J. J. Wallman and J. Emerson, Noise tailoring for scalable quantum computation via randomized compiling, *Phys. Rev. A* **94**, 52325 (2016).
- [36] N. Ezzell, B. Pokharel, L. Tewala, G. Quiroz, and D. A. Lidar, Dynamical decoupling for superconducting qubits: A performance survey, *Physical Review Applied* **20**, 10.1103/physrevapplied.20.064027 (2023).
- [37] R. Majumdar, P. Rivero, F. Metz, A. Hasan, and D. S. Wang, Best practices for quantum error mitigation with digital zero-noise extrapolation (2023).
- [38] Q. Sun, T. C. Berkelbach, N. S. Blunt, G. H. Booth, S. Guo, Z. Li, J. Liu, J. D. McClain, E. R. Sayfutyarova, S. Sharma, S. Wouters, and G. K. L. Chan, Pyscf: the python-based simulations of chemistry framework, *Wiley Interdisciplinary Reviews: Computational Molecular Science* **8**, 10.1002/wcms.1340 (2018), publisher Copyright: © 2017 Wiley Periodicals, Inc.
- [39] M. Nusspickel, B. Ibrahim, and G. H. Booth, Effective reconstruction of expectation values from ab initio quantum embedding, *Journal of Chemical Theory and Computation* **19**, 2769 (2023).
- [40] A. Javadi-Abhari, M. Treinish, K. Krsulich, C. J. Wood, J. Lishman, J. Gacon, S. Martiel, P. D. Nation, L. S. Bishop, A. W. Cross, B. R. Johnson, and J. M. Gambetta, Quantum computing with qiskit (2024).
- [41] Q. Community, Qiskit addon for obp (optimization for basis primitives) (2024), retrieved 2024.
- [42] M. AbuGhanem, Ibm quantum computers: Evolution, performance, and future directions (2024).
- [43] C. Piveteau and D. Sutter, Circuit knitting with classical communication, *IEEE Transactions on Information Theory* **70**, 2734 (2024).
- [44] L. Clinton, J. Bausch, and T. Cubitt, Hamiltonian simulation algorithms for near-term quantum hardware, *Nature Communications* **12**, 4989 (2021).
- [45] K. Setia and J. D. Whitfield, Bravyi-kitaev superfast simulation of electronic structure on a

- quantum computer, *The Journal of Chemical Physics* **148**, 10.1063/1.5019371 (2018).
- [46] A. Miller, Z. Zimborás, S. Knecht, S. Maniscalco, and G. García-Pérez, Bonsai algorithm: Grow your own fermion-to-qubit mappings, *PRX Quantum* **4**, 30314 (2023).
- [47] M. Chiew and S. Strelchuk, Discovering optimal fermion-qubit mappings through algorithmic enumeration, *Quantum* **7**, 1145 (2023).
- [48] E. van den Berg and K. Temme, Circuit optimization of hamiltonian simulation by simultaneous diagonalization of pauli clusters, *Quantum* **4**, 322 (2020).
- [49] A. Tranter, P. J. Love, F. Mintert, and P. V. Coveney, A comparison of the bravyi–kitaev and jordan–wigner transformations for the quantum simulation of quantum chemistry, *Journal of Chemical Theory and Computation* **14**, 5617 (2018), doi: 10.1021/acs.jctc.8b00450.

Appendix A QUANTUM CHEMISTRY SIMULATIONS ON QUANTUM COMPUTERS

The starting point for Hamiltonian simulation is the electronic structure Hamiltonian. Specifically, we use the Fermionic Hamiltonian in the second quantized form:

$$H_f = \sum_{ij}^M h_{ij} \hat{a}_i^\dagger \hat{a}_j + \sum_{ijkl}^M h_{ijkl} \hat{a}_i^\dagger \hat{a}_j^\dagger \hat{a}_k \hat{a}_l$$

where the summation is performed over the active space size, with h_{ij} and h_{ijkl} representing the one- and two-electron integrals of the operators projected into a given basis set, respectively. The \hat{a}_i^\dagger and \hat{a}_i are Fermionic creation and annihilation operators, respectively. To perform Hamiltonian simulations using quantum computers, any given Hamiltonian needs to be converted to a suitable fermionic-to-qubit mapping given as follows:

$$H_q = \sum_{k=1}^K c_k \hat{P}_k$$

where c_k denotes the coefficient, and \hat{P}_k are the tensor products of Pauli matrices, further called ‘Pauli strings’ (or ‘Pauli words’), acting on N qubits:

$$\hat{P}_k = \hat{p}_{1k} \otimes \hat{p}_{1k} \otimes \dots \otimes \hat{p}_{Nk}$$

where $\hat{p}_{1k} \in \{I, \hat{\sigma}_x, \hat{\sigma}_y, \hat{\sigma}_z\}$, with I denoting identity matrix, and σ_i representing the Pauli matrices. To shorten the descriptions, more efficient notation is often used with just the X , Y , Z , and I letters with tensor product signs omitted. There are various qubit mapping methods for chemistry problems such as Jordan-Wigner or Bravyi–Kitaev and alternative methods that consider the device connectivity such as the Bonsai algorithm [46]. It is important to note that efficient fermionic-to-qubit mappings are also key to achieving shallower circuits as efficient mappings not only consider the structure of the problem but also factor in the connectivity of the QPU architecture. This work focuses on simulating the time evolution of a given observable of the chosen system. Quantum computing is utilized to simulate the time-evolved state of the system to a given point in time and finally measuring the expectation value with the appropriate measurement operator. By choosing the Schrödinger representation, the evolved state $\psi(t)$ can be calculated by operating the initial state at time $t_0 = 0$ with the time evolution operator $U(t)$ as given by:

$$|\psi(t)\rangle = U(t)|\psi(t_0)\rangle$$

where:

$$U(t) = e^{-iHt}$$

The evolution operator above in exponent form is one of the possible solutions of the time-dependent Schrödinger equation. Finally, the observable of choice for the system needs to be prepared as a measurement operator \hat{O} in the qubit mapped form. To recreate the time evolution curve of the given observable, its expectation value needs to be estimated over different times t :

$$\langle \psi(t) | \hat{O} | \psi(t) \rangle$$

In the simplest case of energy time evolution, the observable is the same qubit-mapped Hamiltonian used in the time evolution operator. Other observables can be defined to more effectively predict the molecule reactivity [4].

In this paper, we leverage PF decomposition to implement real-time quantum system evolution as described in Appendix B.

Appendix B PRODUCT FORMULAS

The most straightforward method to simulate real-time evolution of quantum systems is to encode the initial state of the simulated system into qubit states (using the same qubit mapping scheme as for the transformation of Hamiltonian from fermionic to qubit mapped form) and evolve them with the time evolution operator as the direct exponentiation of Hamiltonian terms using Product Formulas (PF) approximations, also called Trotter formulas or Trotter-Suzuki decompositions. This way, to recreate the observable trajectory, a series of subexperiments is conducted to estimate the expectation value at a set of time points. In each subexperiment the initial state is encoded, then the time evolution operator is applied to transform the state to a given time point, and finally, the observable expectation value is measured. A high-level scheme of such subexperiment’s quantum circuit is shown in Figure 10.

The challenge lies in the effective and accurate preparation of the time evolution operator. The Product Formulas are the way to approximate the operator so that it can be applied on QPUs. In general, terms in the qubit mapped Hamiltonian H_q don’t commute, which

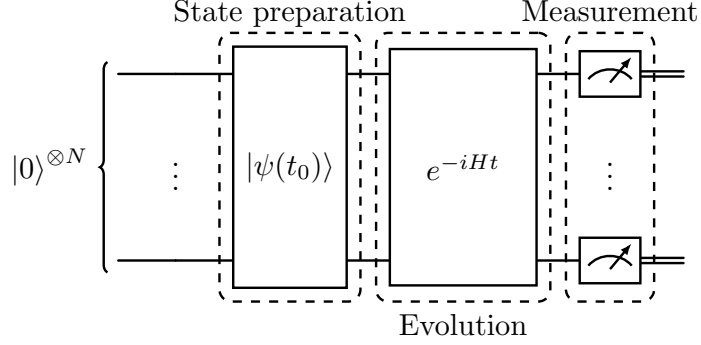


FIG. 10: *Scheme of the real-time evolution simulation circuit*

means, that the time evolution operator can't be prepared as a product of operators of each Pauli term:

$$e^{-iHqt} = e^{-i(c_1\hat{P}_1 + \dots + c_k\hat{P}_k)t} \neq e^{-i(c_1\hat{P}_1)t} \dots e^{-i(c_k\hat{P}_k)t}$$

The most straightforward approximation is the first-order PF, called Lie-Trotter product formula:

$$e^{-i(c_1\hat{P}_1 + \dots + c_k\hat{P}_k)t} = \lim_{n \rightarrow \infty} \left(e^{\frac{-i(c_1\hat{P}_1)t}{n}} \dots e^{\frac{-i(c_k\hat{P}_k)t}{n}} \right)^n$$

Where n , the so-called Trotter number or number of Trotter steps, is an arbitrary number adjusting the level of approximation for the physical implementation on QPUs.

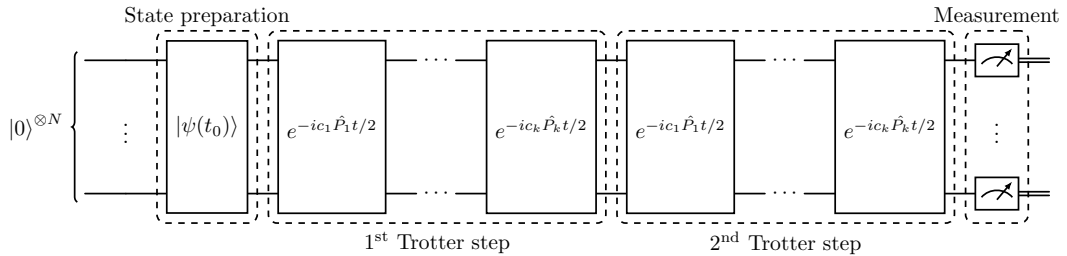


FIG. 11: *Time evolution simulation circuit approximated with two Trotter steps*

Higher order formulas were proposed to decompose exponent with the sum of terms more efficiently – that means with a faster decrease in error with a number of Trotter steps so that

the shallower circuit can be made to express the same problem with the same accuracy or the circuit of the same depth with better accuracy than the one obtained from lower-order formulas. A good overview of those is in [10].

Appendix C PAULI STRINGS EXPONENTIATION GATE COST

To understand the gate complexity of the circuits produced by PFs, the application of each exponentiated Pauli term operator on the quantum circuit needs to be considered. Each arbitrary term can be applied exactly on a gate-based quantum computer.

For instance, let's take the term $\hat{P} = \hat{\sigma}_z \otimes \hat{I} \otimes \hat{\sigma}_x \otimes \hat{\sigma}_y \otimes \hat{\sigma}_z$, with some coefficient c_i . First, the term is diagonalized by changing the basis to the computational one, on the qubits, where $\hat{\sigma}_x$ and $\hat{\sigma}_y$ are applied. Now, all the qubits influenced by the term (i.e. with respective non-identity matrix in the term) are ready to apply the term in the computational basis. Then the parity check is performed, since for terms with computational basis vectors, the eigenvalues are determined by the parity of the vector bit strings. The parity check can be done efficiently on QPU with linear connectivity with the 'chain' or 'ladder' of CNOTs, as shown in Figure 12. Then a single R_z rotation is applied depending on the simulated time step and the term's coefficient. The circuit is finalized with the parity check uncomputing and changing back the basis of qubits.

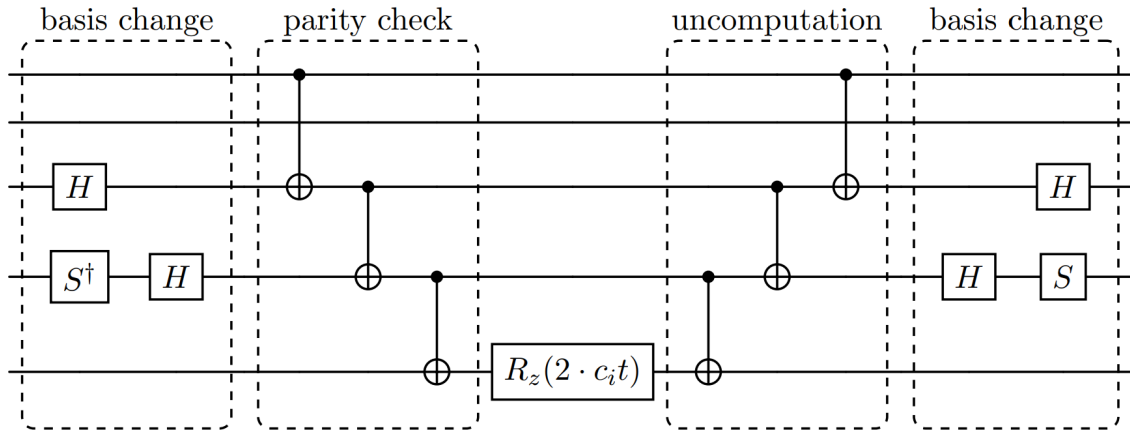


FIG. 12: Example of Pauli string $\hat{\sigma}_z \otimes \hat{I} \otimes \hat{\sigma}_x \otimes \hat{\sigma}_y \otimes \hat{\sigma}_z$ (ZIXYZ) exponentiation on a quantum circuit.

This gives a way to express the exponentiated Pauli terms of a weight w with $2(w - 1)$ CNOT gates and maximally $4w + 1$ single qubit gates. Now, let's consider the real backend case. To make it general, let's consider a backend with linear connectivity and *Clifford*+ R_z basis gate set. Each of the identity operators in the Pauli term, which has a non-identity operator before or after itself, requires 2 swap gates, which in general requires 3 CNOT gates to decompose each as shown in Figure 13.

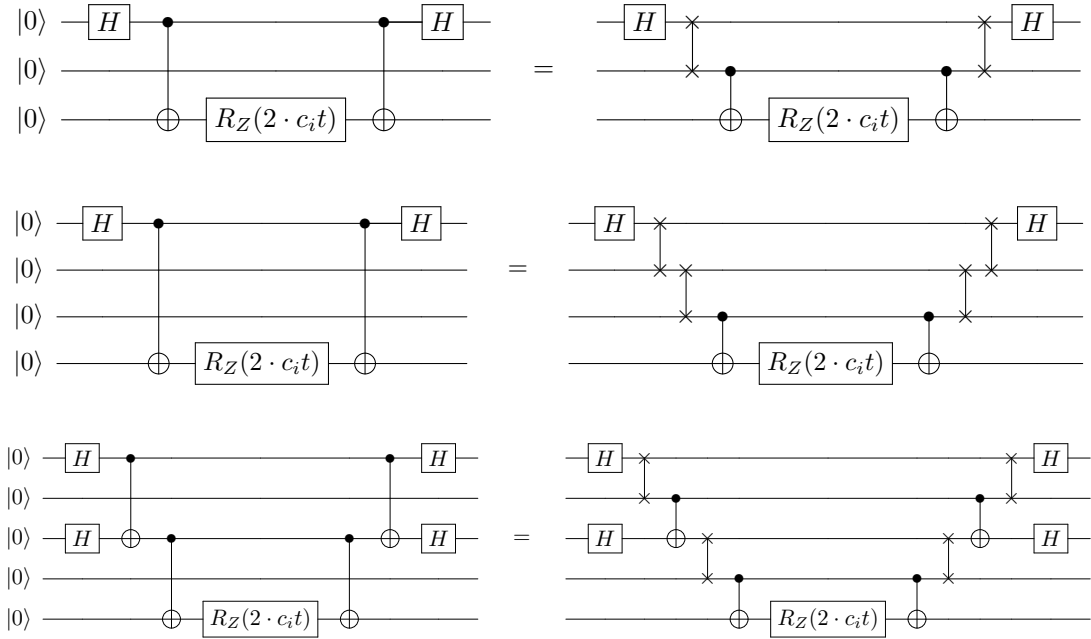


FIG. 13: *Example of Pauli strings with identity matrices exponentiation on a quantum circuit. Terms respectively from the top are XIZ, XIIZ, XIXIX.*

That means, that the final circuit depth depends on the structure of the Pauli term, not only its weight. In the worst-case scenario, the 2-qubit gate complexity is $O(n) = 6(n - 1) + 2$ where n is a number of qubits.

Further optimizations are possible. To name a few: the simplest would be cancellation of the gates from the adjacent terms sections in the circuit. If the single-term section ends with e.g. a Hadamard or CNOT gate and the other section begins with them on the same qubits, those gates can be canceled out. This technique is usually automatically applied by the transpiler. A more advanced method is simultaneous diagonalization [48], i.e. application group of the commuting terms using fewer gates, than it would be with the sequential

exponentiation of the terms. For this method to be visibly effective, the commuting terms need to be grouped together, changing radically the order of the original terms sequence, which may strongly influence the final state for the small number of Trotter steps. In the end, promising results in circuit reduction were also shown in this work [11].

Appendix D QUBIT MAPPING COMPARISON

During testing methods reducing circuits, the generic qubit mapping methods were checked: Jordan-Wigner (JW), Bravyi-Kitaev (BK), and Parity mappings. By comparing circuits in Figure 14, for full Hamiltonian from generic Trotterization with 1 Trotter steps, there are no significant differences between those 3 for <30 qubits, from where BK started to produce shallower circuits. It agrees with a broader study on the quantum chemistry dataset comparing JW to BK [49].

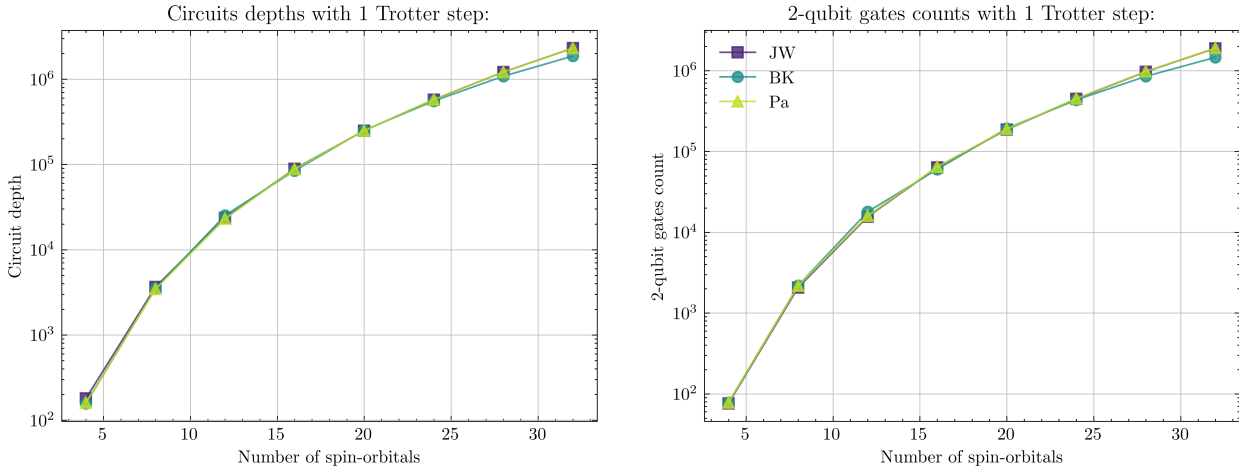


FIG. 14: *Circuit depth and 2-qubit gate comparison on circuits yielded by first-order 1 Trotter step PF with Clifford + R_z gates only for Jordan-Wigner (JW), Bravyi-Kitaev (BK) and Parity (Pa) mappings.*

Since the focus in this work is on low number of qubits regimes, the JW mapping was chosen. All previous results in the main part of the paper were produced with it. Additionally, to check potential differences between the mappings for methods reducing circuits from Trotterization, all the results were generated for BK and Parity mappings as well and shown in the appendix F.

Appendix E CIRCUIT DEPTH REDUCTION METHODS

A Hamiltonian terms truncation

The number of terms in the qubit mapped Hamiltonian linearly contributes to the circuit depth in the first-order PF, which makes it challenging to both simulate and run on the real devices with each increase in the active space size of the simulated system. For the targeted covalent drugs use case, similarly to most of the use cases leveraging time evolution dynamics of the quantum chemistry systems, only the arbitrary initial time range of the observable trajectory is taken into consideration. That means that Hamiltonian terms with small coefficients won't influence noticeably the final observable within the chosen time range and can be neglected. Let's show it on single term single-qubit Hamiltonian $\hat{H}_p = c_H \hat{P}_H$ example and single term, single-qubit observable $\hat{A} = \hat{P}_A$. For simplicity reasons, let's consider $\hat{P}_H = \hat{\sigma}_x$ and $\hat{P}_A = \hat{\sigma}_z$.

For the state $|\psi\rangle$ and observable \hat{A} , the expectation value of the \hat{A} is defined as:

$$\langle \hat{A} \rangle = \langle \psi | \hat{A} | \psi \rangle$$

The measured state is time-evolved state from arbitrarily chosen initial state $|\psi_{init}\rangle$:

$$|\psi\rangle = e^{i\hat{H}_p t} |\psi_{init}\rangle = e^{i(c_1 \hat{\sigma}_x)t} |\psi_{init}\rangle$$

After unrolling the exponent into power series by the definition, and grouping even and odd power terms, the formula looks like:

$$e^{i(c_1 \hat{\sigma}_x)t} = \sum_{j=0}^{\infty} \frac{(-i c_1 t)^j}{j!} \hat{\sigma}_x^j = \sum_{j=0}^{\infty} \frac{(-1)^j (c_1 t)^{2j}}{(2j)!} \hat{I} + \sum_{j=0}^{\infty} \frac{-(-1)^j (c_1 t)^{2j+1}}{(2j+1)!} \hat{\sigma}_x = \cos(c_1 t) \hat{I} - i \sin(c_1 t) \hat{\sigma}_x$$

And with the representation in the computational basis:

$$|\psi_{init}\rangle = \begin{bmatrix} \alpha_0 \\ \alpha_1 \end{bmatrix}$$

$$e^{i(c_1 \hat{\sigma}_x)t} = \cos(c_1 t) \hat{I} - i \sin(c_1 t) \hat{\sigma}_x = \begin{bmatrix} \cos(c_1 t) & -i \sin(c_1 t) \\ -i \sin(c_1 t) & \cos(c_1 t) \end{bmatrix},$$

what is exactly $R_x(2 \cdot c_1 t)$, which is applied in the circuit.

$$|\psi\rangle = \begin{bmatrix} \cos(c_1 t) & -i \sin(c_1 t) \\ -i \sin(c_1 t) & \cos(c_1 t) \end{bmatrix} \begin{bmatrix} \alpha_0 \\ \alpha_1 \end{bmatrix} = \begin{bmatrix} \cos(c_1 t) \alpha_0 - i \sin(c_1 t) \alpha_1 \\ -i \sin(c_1 t) \alpha_0 + \cos(c_1 t) \alpha_1 \end{bmatrix}$$

That gives the formula for the expectation value:

$$\langle \hat{A} \rangle = \langle \psi | \hat{\sigma}_z | \psi \rangle$$

$$\langle \hat{A} \rangle = \begin{bmatrix} \cos(c_1 t) \alpha_0^* + i \sin(c_1 t) \alpha_1^* & i \sin(c_1 t) \alpha_0^* + \cos(c_1 t) \alpha_1^* \end{bmatrix} \begin{bmatrix} 1 & 0 \\ 0 & -1 \end{bmatrix} \begin{bmatrix} \cos(c_1 t) \alpha_0 - i \sin(c_1 t) \alpha_1 \\ -i \sin(c_1 t) \alpha_0 + \cos(c_1 t) \alpha_1 \end{bmatrix}$$

$$\langle \hat{A} \rangle = \cos(2c_1 t) (|\alpha_0|^2 - |\alpha_1|^2) + i \sin(2c_1 t) (\alpha_0 \alpha_1^* - \alpha_0^* \alpha_1)$$

that means the period of the observable's expectation value is π/c_1 , so the higher the terms' coefficient, the higher the frequency of a an observable potential variation induced by the term. Now, to assess if the term in Hamiltonian can be skipped, the maximum change induced by the term to the observable needs to be accessed:

$$\frac{d\langle \hat{A} \rangle}{dt} = -2c_1 (\sin(2c_1 t) (|\alpha_0|^2 - |\alpha_1|^2) - i \cos(2c_1 t) (\alpha_0 \alpha_1^* - \alpha_0^* \alpha_1))$$

Since $|\alpha_0|^2 + |\alpha_1|^2$ needs to be 1, there expression simplify to:

$$\frac{d\langle \hat{A} \rangle}{dt} = -2c_1 (\sin(2c_1 t) (1 - 2|\alpha_1|^2) - i \cos(2c_1 t) (\alpha_0 \alpha_1^* - \alpha_0^* \alpha_1))$$

Then, to calculate the maximum value with respect to the initial state, the global phase can be neglected and the α_0 may be chosen as the real amplitude. That means, that the second term will yield maximum absolute value if the α_1 will be imaginary. This condition is fulfilled by the initial states across the Z-Y axes plane of the Bloch sphere – perpendicular to the X axis. Those two specifications allow to yield the formula dependent only on the single amplitude:

$$\max_{(\alpha_0, \alpha_1)} \left(\left| \frac{d\langle \hat{A} \rangle}{dt} \right| \right) = \max_{\alpha_1} \left(\left| 2c_1 (\sin(2c_1 t) (1 - 2|\alpha_1|^2) \pm 2 \cos(2c_1 t) \sqrt{1 - \text{Im}(\alpha_1)^2} \text{Im}(\alpha_1)) \right| \right)$$

First term gives the largest value $2c_1$ (for $t = \frac{\pi}{4c_1} (1 + 2n)$) for the $|\alpha_1|^2 \in [0, 1]$, the second gives the same largest value (for $t = \frac{n\pi}{2c_1}$) for $\alpha_1 \in \{\frac{i}{\sqrt{2}}, \frac{-i}{\sqrt{2}}\}$. The numerical evaluation also yielded largest value $2c_1$ for the possible space of α_1 and t :

This way, the worst-case scenario of the observable expectation variation $d\langle \hat{A} \rangle$ from the Hamiltonian's term with coefficient c_1 for a given time range dt is:

$$\max(d\langle \hat{A} \rangle) = 2c_1 dt$$

Let's generalize this example to Hamiltonian with any number of terms acting on many qubits. Based on this formula, the truncation algorithm may be set, cutting off the given

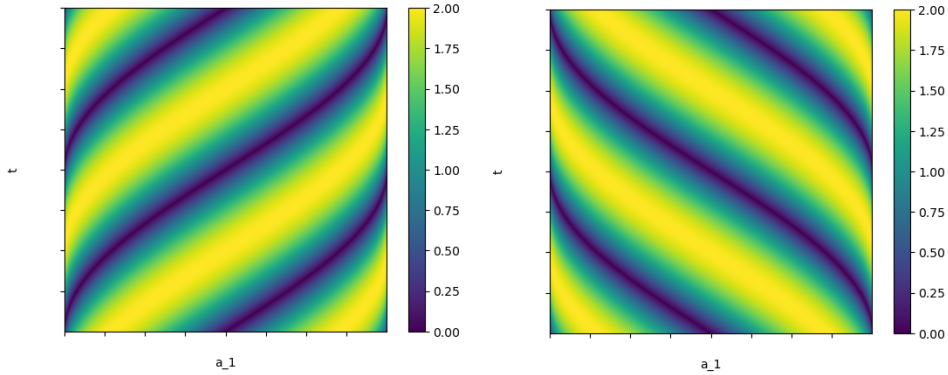


FIG. 15: $\frac{d\langle\hat{A}\rangle}{dt}$ numerical evaluation from t and α_1 amplitude.

Hamiltonian's terms. The threshold will be set for the coefficients c_0 , below which the terms will be neglected as they shouldn't influence any observable expectation value more than given acceptable value $\epsilon_{d\langle\hat{A}\rangle}$:

$$c_0 = \frac{\epsilon_{d\langle\hat{A}\rangle}}{2dt}$$

For example, for the $\epsilon_{d\langle\hat{A}\rangle} = 1\%$ and time range of 0-10 time (a.u.), the acceptable threshold is $c_0 = 0.0005$. A schematic representation of the truncation algorithm through pseudocode is shown in Figure 16 below.

Algorithm 1 *Basic Truncation Algorithm. Hamiltonian terms truncation algorithm pseudocode. H_q denotes qubit mapped Hamiltonian, c_k is the coefficient of term P_k , and c_0 is the absolute value coefficient threshold.*

```

1: procedure TRUNCATE_HAMILTONIAN( $H_q, c_0$ )
2:    $H_{trunc} \leftarrow \{\}$ 
3:   for each term  $(c_i, H_i)$  in Hamiltonian do
4:     if  $|c_i| > c_0$  then
5:       Append  $(c_i, H_i)$  to  $H_{trunc}$ 
6:     end if
7:   end for
8:   return  $H_{trunc}$ 
9: end procedure

```

FIG. 16: Pseudocode for a basic implementation of Hamiltonian terms truncation algorithm.

B Qubit tapering

Qubit tapering is the technique leveraging the Z_2 symmetries in the molecular Hamiltonians to perform the Hamiltonian simulation using fewer qubits and in some cases with shallower circuits. Fundamentally, the original qubit Hamiltonian \hat{H}_q is transformed as:

$$\hat{H}_q = \sum_{k=1}^K c_k \hat{P}_k$$

into new Hamiltonian \hat{H}'_q , which will have the same eigenvalues as \hat{H}_q , using unitary operator \hat{U} :

$$\hat{H}'_q = \hat{U}^\dagger \hat{H}_q \hat{U} = \sum_{k=1}^K c'_k \hat{P}'_k$$

but with each of the terms \hat{P}'_k containing the same Paulis acting on a subset of qubits. To illustrate it, let's take:

$$\hat{H}' = \hat{\sigma}_x \otimes \hat{\sigma}_z - \hat{I} \otimes \hat{\sigma}_z$$

All the terms apply on the second qubit the $\hat{\sigma}_z$ operator. In that case, the Hamiltonian can be rewritten as:

$$\hat{H}' = \left(\hat{\sigma}_x \otimes \hat{I} - \hat{I} \otimes \hat{I} \right) \hat{I} \otimes \hat{\sigma}_z$$

yielding two tapered Hamiltonians with the eigenvalues of $\hat{\sigma}_z$ as the prefactor:

$$\hat{H}_{tapered} = \pm 1 (\hat{\sigma}_x - \hat{I})$$

with the Paulis acting on the first qubit only. This way, for two eigenvalues from each of the 1-qubit $\hat{H}_{tapered}$, there are in total 4 eigenvalues being the eigenvalues of the 2-qubit \hat{H}'_q . 2 qubits are ‘tapered’ out and the cost of the Hamiltonian exponentiation on the circuit for the potential simulation is reduced. The challenge lies in finding the original Hamiltonian \hat{H}_q symmetries, and then the preparation of \hat{H}'_q from \hat{H}_q by leveraging found symmetries to taper as much qubits as possible. Methods for this were described first in the [30], with the extension in [31]. For the results in this paper, the Qiskit’s Z2Symmetries class was used with the original tapering method implementation [30].

C Clifford Decomposition and Transformation (CDAT)

Clifford Decomposition and Transformation (CDAT) is the procedure described in [29]. During the simulating circuit creation, given steps are taken iteratively: taking the Pauli term $c_k \hat{P}_k$ from qubit mapped Hamiltonian with evolution time t , exponentiate them on the circuit $\hat{V}_k(\theta_k) = e^{-i\theta_k \hat{P}_k}$, where $\theta_k = c_k t$, and then using a few quantum gates identities the circuit is transformed in such a way, that it can be decomposed into Clifford part \hat{C}_k (containing only Clifford gates, hence non-parametrized) and non-Clifford part $\hat{U}_k(\theta_k)$ (containing Clifford and non-Clifford gates) giving $\hat{V}_k(\theta_k) = \hat{C}_k \hat{U}_k(\theta_k)$, so the non-Clifford part is applied in the decomposed circuit first. Then the Clifford gates \hat{C}_k are taken from the decomposed circuit and used to transform the remaining Paulis and all the measurement operators. Since, the \hat{C}_k is already applied, the non-Clifford part $\hat{U}_k(\theta_k)$ can be applied to the already existing circuit from previous terms, and the process is repeated for the rest of the Paulis in the Hamiltonian. Following supplementary materials of [29], here's the illustrative example of 3 terms circuit transformation:

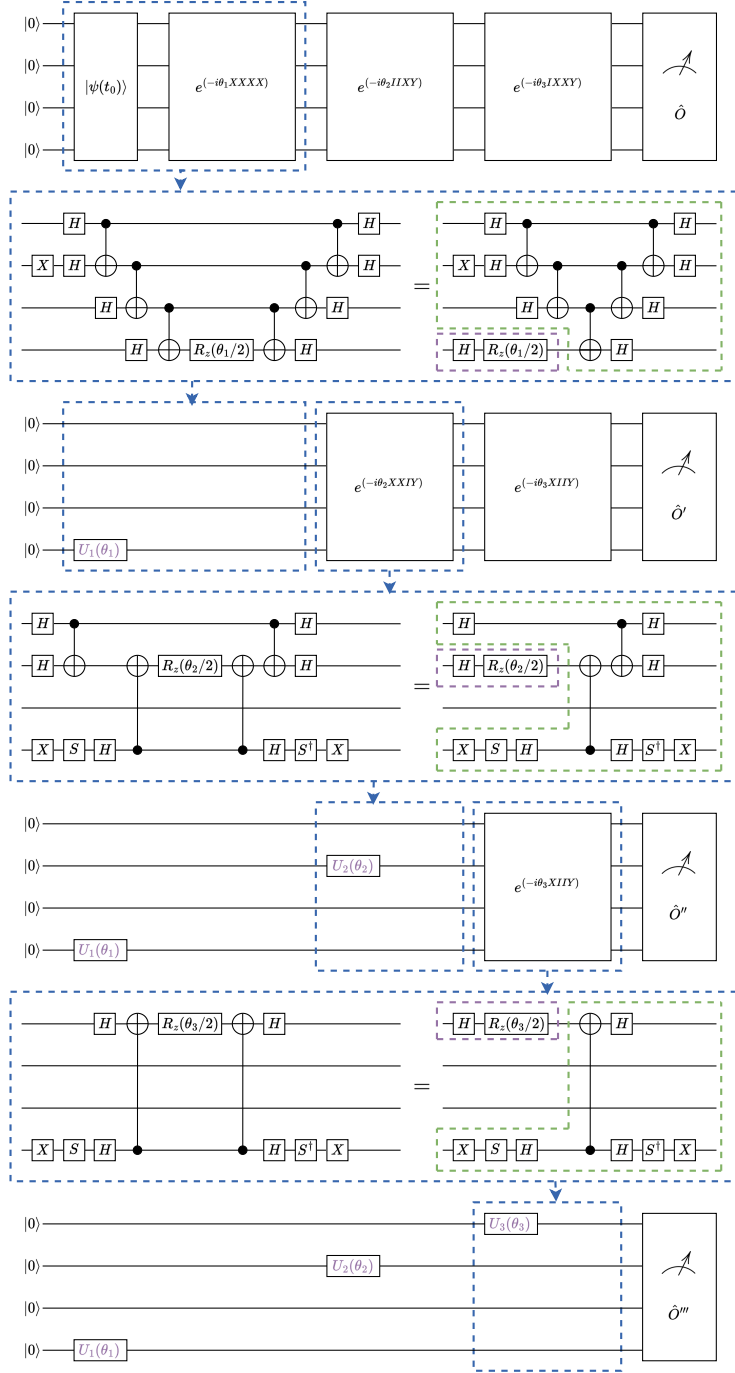


FIG. 17: CDAT 4 qubits representation example. Adapted and redrawn from supplementary information of [29].

Appendix F DETAILED CIRCUIT REDUCTION RESULTS

A Clifford Decomposition and Transformation (CDAT)

CDAT gives similar, systematic reduction both for circuit depth and 2-qubit gates.

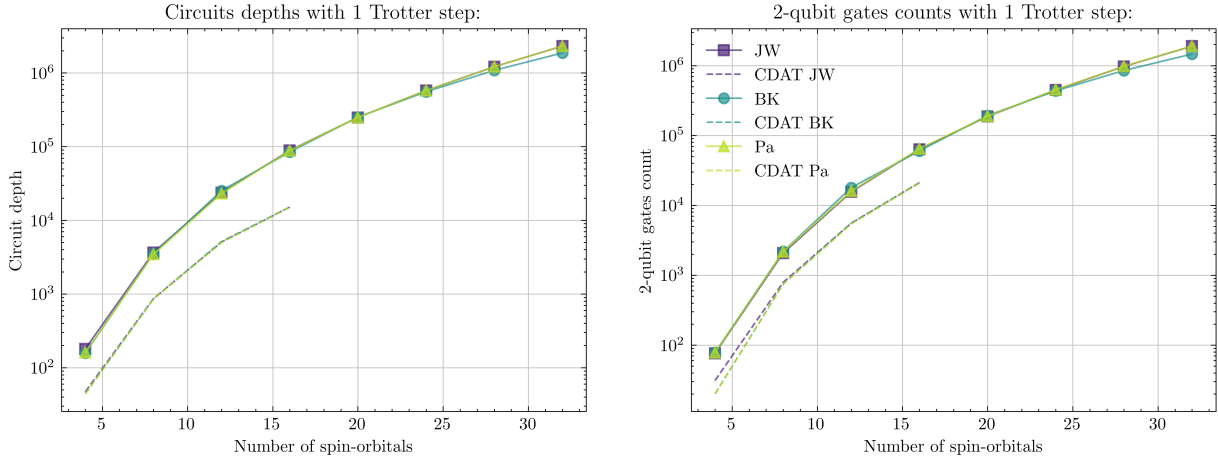


FIG. 18: *Circuit depths and number of 2-qubit gates comparison with and without CDAT applied for different qubit mappings.*

B Qubit Tapering

All results for qubit tapering are taken as a mean from all subexperiments. In all cases, the number of terms stayed on a similar level both in the Hamiltonian and the measurement operator. The circuit depth results vary in the small active space sizes for different qubit mappings. Besides that, the depths from different mappings are close to each other.

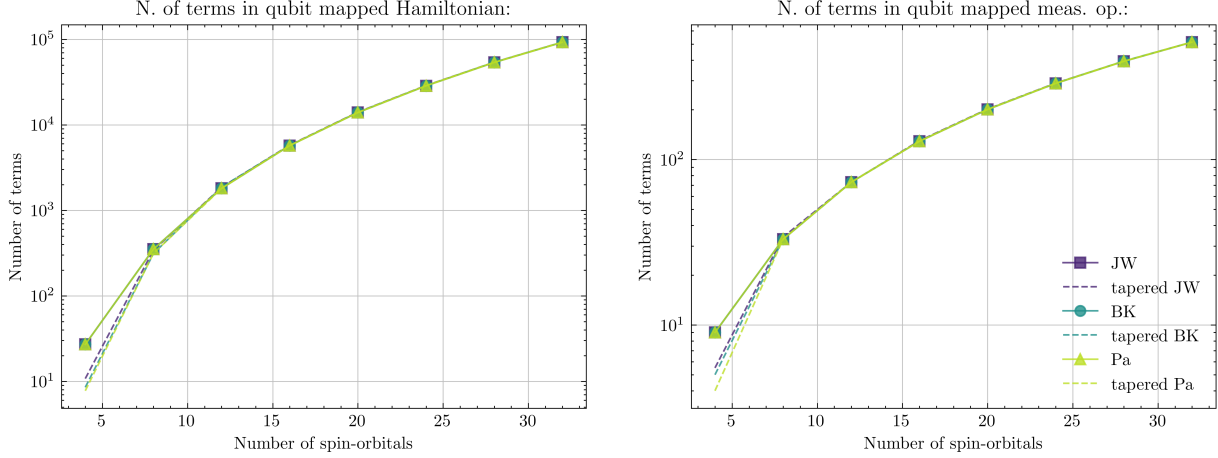


FIG. 19: *Number of terms in Hamiltonian and measurement observable comparison with and without qubit tapering applied for different qubit mappings.*

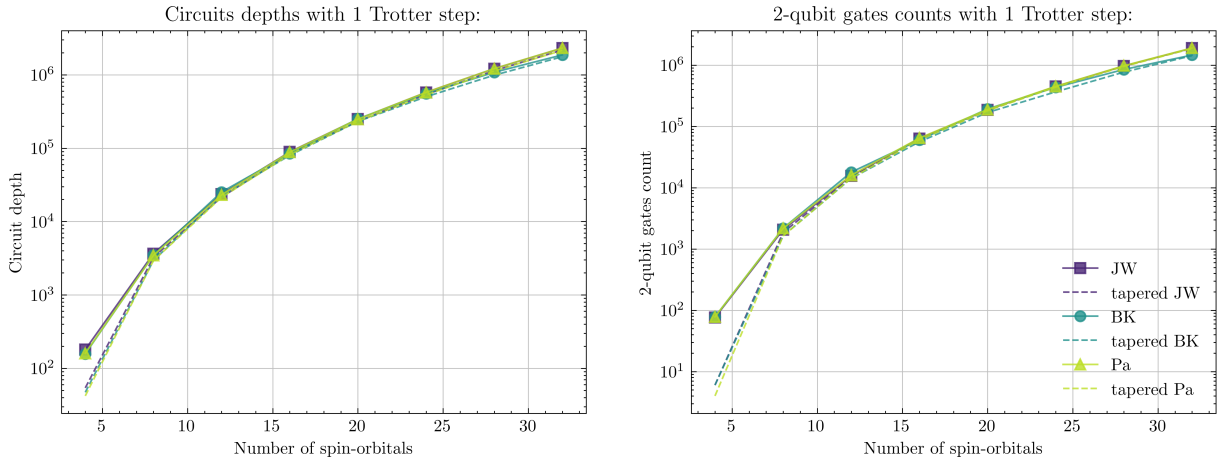


FIG. 20: *Circuit depths and number of 2-qubit gates comparison with and without qubit tapering applied for different qubit mappings.*

C Comparison of the combinations

Additionally, the combination of the tapering and CDAT (tapering applied first) was checked for potential improvements. The two plots below show the comparison to CDAT or qubit tapering applied only. A combination of this too yields significantly smaller circuits, than just the tapering, but in comparison to CDAT only, it's a little bit worse for 8+ qubits.

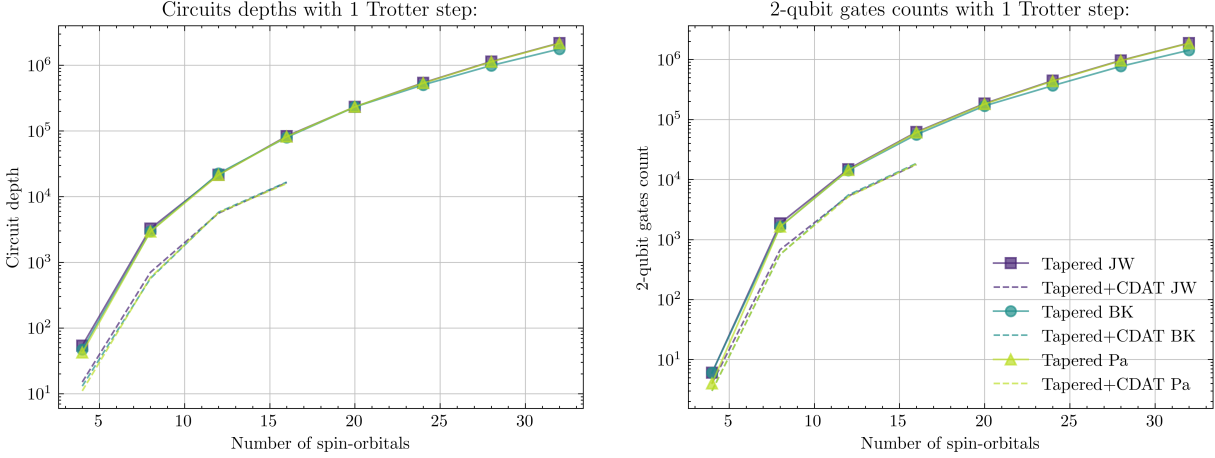


FIG. 21: *Circuit depths and a number of 2-qubit gates comparison with qubit tapering applied only and with qubit tapering and CDAT applied for different qubit mappings.*

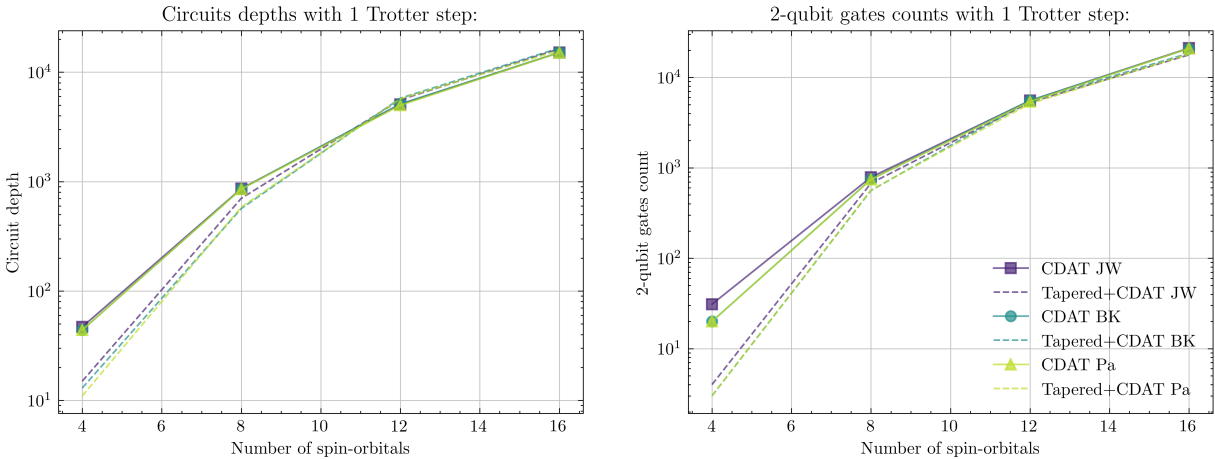


FIG. 22: *Circuit depths and a number of 2-qubit gates comparison with CDAT applied only and with qubit tapering and CDAT applied for different qubit mappings.*

Since qubit tapering didn't induce any reduction both applied alone and with CDAT it wasn't include in the real backend runs or any simulations in this paper.

Appendix G DISTRIBUTION OF HAMILTONIAN TERMS' COEFFICIENT EXAMPLE

A representative example of the distribution of the absolute values of the term's coefficient in 12 qubits example is shown in Figure 23 with the arbitrary coefficients threshold to limit any observable expectation value error to $\epsilon_{d(\langle \hat{A} \rangle)} = 2\%$ for the max. time 14 (a.u.). In this example, only 467 of the default 1807 terms (25.84%) need to be included for the accurate simulation.

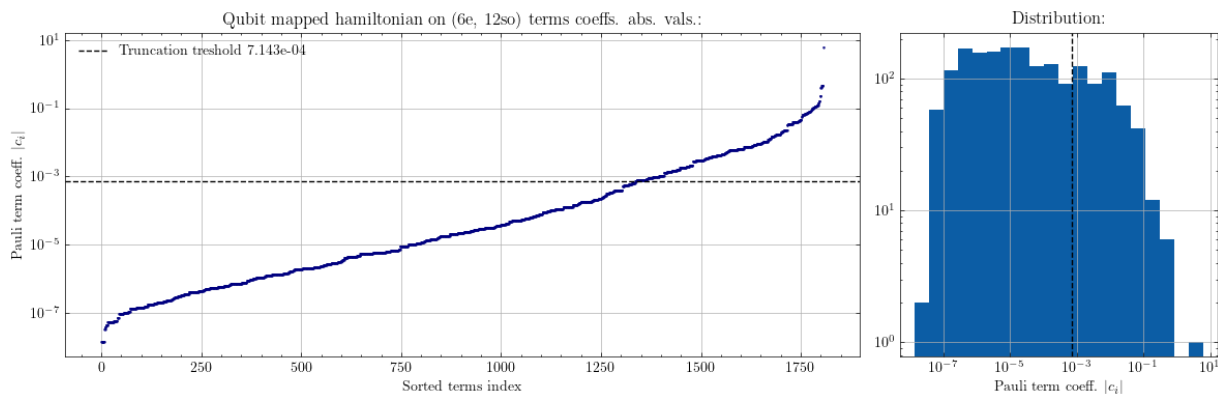


FIG. 23: *Distribution of the absolute values of the term's coefficient of exemplary molecule with active space (6e, 12so) on 12 qubits with marked coefficients threshold to limit any observable exp. val. error to $\epsilon_{d(\langle \hat{A} \rangle)} = 2\%$ for the max. time 14 (a.u.)*

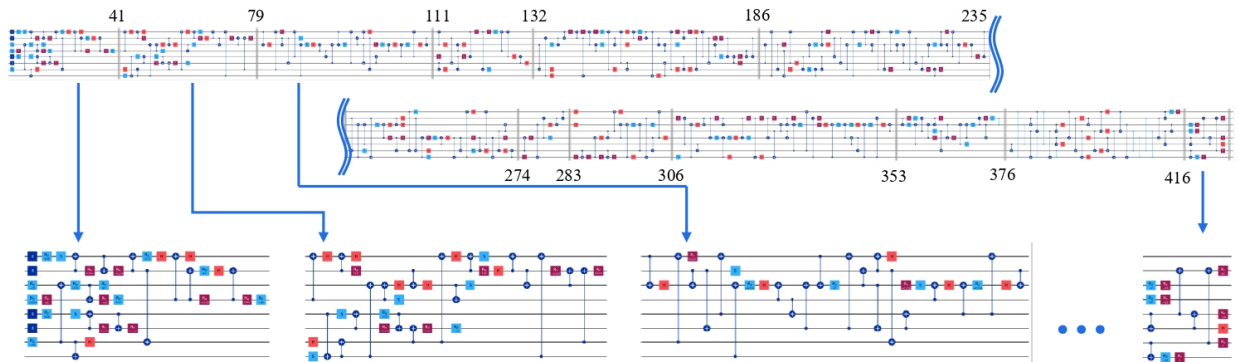


FIG. 24: *Decomposition of 8 qubits circuit for the time point 100 into 13 blocks of size from 9 to 55 gates before the transpilation to device. Numbers indicate the gate count at which barriers are inserted.*

Appendix H DETAILED RESULTS OF QPU RUNS WITH MIDDLEWARE

The partitioning strategy within OE is based on multiple variables including circuit structure, layout mapping, sub-block entanglement, and fidelity of its execution on a noisy QPU.

In the case of the quantum circuits used for the energy calculation at time step 100, the full circuit consisting of 431 gates is partitioned into $N_{blocks} = 13$ sub-blocks, as can be seen in Figure 24. Here the barriers are added at the depths of 41, 79, 111, 132, 186, 235, 274, 283, 306, 353, 376, and 416. This results in sub-circuits of variable size: from 9 to 55 gates before transpilation to the device.

The execution of the full circuit on a QPU is performed as $N_{sampling} \times n_{blocks}$ QPU executions of the modified sub-block circuits, with an overhead of $N_{sampling}$ related to sampling the initial state and internal circuit structure, related to specifics of the method. For the problem circuits at hand $N_{sampling} = 600$. Each execution includes the application of custom noise mitigation and suppression pipeline involving Dynamical Decoupling, Pauli Twirling, and Readout Error Mitigation. With $N_{twirls} = 8$ twirled circuit copies this sums up to 4800 circuit executions per sub-block, however, we keep the overall shot budget for a twirled set

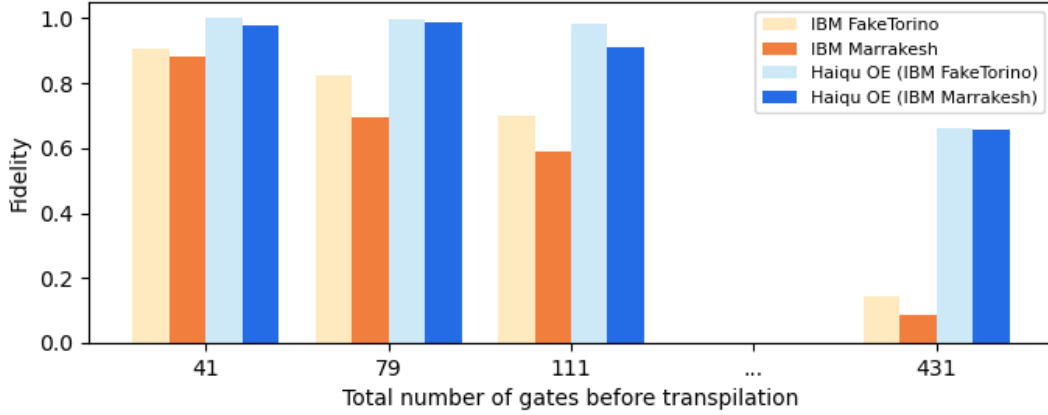
of 8 circuits $N_{shots} = 10000$.

We test our approach on noisy IBM devices using the Heron R2 architecture - the actual IBM Marrakesh QPU, and the IBM FakeTorino simulator, which provides the layout and a high-fidelity noise model of a Heron architecture.

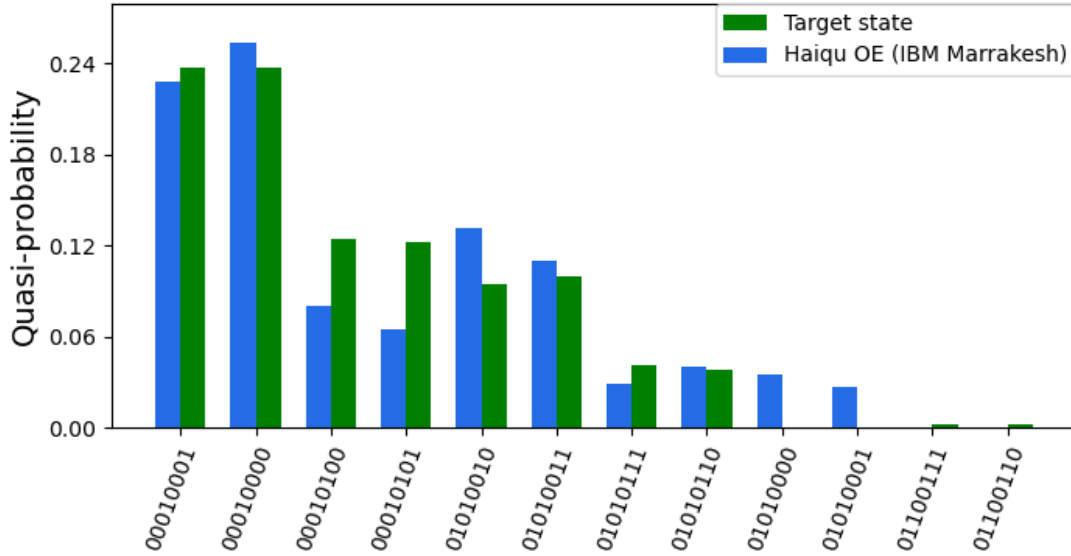
Given the block nature of the method, we can reconstruct the state at each intermediate barrier. In Figure 25 a) we plot the intermediate fidelities at different steps for the distributions sampled from the noisy devices with and without Haiqu's OE approach against the ideal simulation (which is still possible at this qubit scale). We observe that the method performs qualitatively similarly on both real and simulated QPU, resulting in fidelity values significantly higher than the direct execution of the circuit.

In Figure 25 b) we compare the sampled bitstrings distribution for the intermediate state at gate 111 obtained on the IBM Marrakesh QPU with our method to the one obtained from executing on an ideal simulator.

Due to the limited hardware QPU accessibility and overhead of the method, to reconstruct the state at the end of the full circuit, we performed part of the execution batches on the actual IBM Marrakesh QPU while some of the intermediate blocks are executed on noisy IBM FakeTorino simulator. The reported last step fidelity and energy values estimation at time steps 1, 39, and 100 are obtained using such a combined approach.



(a)



(b)

FIG. 25: (a) Comparison of the fidelity of the 8 qubit circuit at timestep 100. On the x-axis, the total number of gates before transpilation executed with Haiqu OE is shown, compared to executing the circuit up to the same point with the default setting on QPU (optimization_level=3, dynamical decoupling). (b) The intermediate quasi-probability distributions of the target state at gate number 111 compared to that, measured on IBM Marrakesh using Haiqu OE